AD-A099 984 MISSION RESEARCH CORP LA JOLLA CA F/G 18/3
MEASUREMENT OF THE ELECTRICAL PROPERTIES OF HIGHLY DOSED AIR IN--ETC(U)
OCT 80 J G CHERVENAK, V A VAN LINT DNA001-80-C-0076
UNCLASSIFIED MRC/SD-R-64 DNA-5492T NL

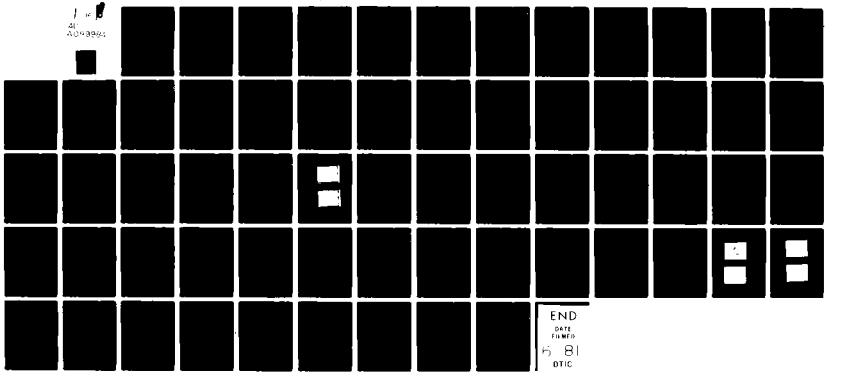

END
DATE FILMED
6 81
DTIC

DNA 5492T

MEASUREMENT OF THE ELECTRICAL PROPERTIES OF HIGHLY DOSED AIR IN THE MILLISECOND REGIME

Mission Research Corporation
P.O. Box 1209
La Jolla, California 92038

24 October 1980

Topical Report for Period 15 January 1980—15 October 1980

CONTRACT No. DNA 001-80-C-0076

APPROVED FOR PUBLIC RELEASE;
DISTRIBUTION UNLIMITED.

THIS WORK SPONSORED BY THE DEFENSE NUCLEAR AGENCY
UNDER RDT&E RMSS CODE B323080464 X99QAXVC30102 H2590D.

Prepared for
Director
DEFENSE NUCLEAR AGENCY
Washington, D. C. 20305

Destroy this report when it is no longer needed. Do not return to sender.

PLEASE NOTIFY THE DEFENSE NUCLEAR AGENCY, ATTN: STTI, WASHINGTON, D.C. 20305, IF YOUR ADDRESS IS INCORRECT, IF YOU WISH TO BE DELETED FROM THE DISTRIBUTION LIST, OR IF THE ADDRESSEE IS NO LONGER EMPLOYED BY YOUR ORGANIZATION.

UNCLASSIFIED

SECURITY CLASSIFICATION OF THIS PAGE (When Data Entered)

17 C301

19 REPORT DOCUMENTATION PAGE

READ INSTRUCTIONS BEFORE COMPLETING FORM

1 REPORT NUMBER: 18 DNA 5492T	2. GOVT ACCESSION NO.: AD-A099984 (9)
3 RECIPIENT'S CATALOG NUMBER	
4 TITLE (and Subtitle): 6 MEASUREMENT OF THE ELECTRICAL PROPERTIES OF HIGHLY DOSED AIR IN THE MILLISECOND REGIME.	5 TYPE OF REPORT & PERIOD COVERED: Topical Report for Period 15 Jan 80 — 15 Oct 80
	6 PERFORMING ORG. REPORT NUMBER: 14 MRC/SD-R-64
7 AUTHOR(s): 1 J.G./Chervenak, V.A.J./van Lint	8 CONTRACT OR GRANT NUMBER(s): 15 DNA 001-80-C-0076
9 PERFORMING ORGANIZATION NAME AND ADDRESS: Mission Research Corporation, P.O. Box 1209, La Jolla, California 92038	10 PROGRAM ELEMENT, PROJECT, TASK AREA & WORK UNIT NUMBERS: 16 Subtask X99QAXVC301-02
11 CONTROLLING OFFICE NAME AND ADDRESS: 11 Director, Defense Nuclear Agency, Washington, D.C. 20305	12 REPORT DATE: 24 October 1980
	13 NUMBER OF PAGES: 62
14 MONITORING AGENCY NAME & ADDRESS (if different from Controlling Office): 12 63	15 SECURITY CLASS (of this report): UNCLASSIFIED
	15a DECLASSIFICATION DOWNGRADING SCHEDULE: N/A

16 DISTRIBUTION STATEMENT (of this Report)

Approved for public release; distribution unlimited.

17 DISTRIBUTION STATEMENT (of the abstract entered in Block 20, if different from Report)

18 SUPPLEMENTARY NOTES

This work sponsored by the Defense Nuclear Agency under RDT&E RMSS Code B323080464 X99QAXVC30102 H2590D.

19 KEY WORDS (Continue on reverse side if necessary and identify by block number)

Highly dosed air
Air conductivity
Electron attachment
Nuclear lightning
Ion-ion recombination

20 ABSTRACT (Continue on reverse side if necessary and identify by block number)

An experiment was performed to measure the conductivity of air after the air had received a megarad dose. The ratio of the electron mobility to the attachment rate and the ratio of the ion mobility to the ion-ion recombination coefficient were found to be the same for highly dosed air and undosed air.

DD FORM 1 JAN 73 1473 EDITION OF 1 NOV 65 IS OBSOLETE

UNCLASSIFIED

SECURITY CLASSIFICATION OF THIS PAGE (When Data Entered)

392797

PREFACE

We acknowledge the considerable assistance of the Sandia Corporation HERMES II staff in providing the radiation sources and dosimetry, and for developing the means to control the firing of the Febetron in the aftermath of a HERMES pulse. We also wish to thank Dennis Breuner and Leo Cotter for design and construction on the electronics.

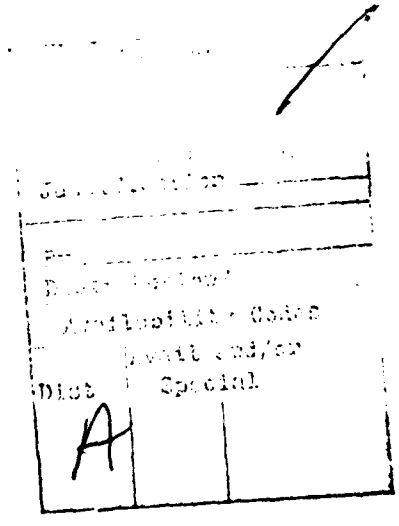

TABLE OF CONTENTS

LIST OF ILLUSTRATIONS

LIST OF TABLES

SECTION 1

INTRODUCTION

The subject of this report is an experiment to measure the electrical properties (electron and ion conductivities) of air that has received a dose on the order of the dose received by air at late times (.1 to 10 m) after a nuclear burst (Ref. 1). The HERMES II facility of Sandia Corporation was used in the electron mode to produce highly dosed air in a ion chamber and a Febetron flash x-ray source was used to reintroduce free electrons into the air at late times in order to measure the electron conductivity.

The electrical conductivity of air is an important parameter in source region EMP calculations. The γ rays from a nuclear burst drive a radially outward flux of Compton electrons, creating a region of positive charge and a resultant electric field directed radially outward. The electric field rapidly attains a saturation value resulting from a balance between the outward flow of Compton electrons and an inward flow of secondary electrons moving in the resultant field. This quasistatic electric field is given by J_K/σ, where J_K is the current of kinetic (Compton) electrons and σ is the conductivity of the air.

Air in the aftermath of a nuclear burst is a chemically different gas than normal, undosed air. The energy deposited in the air, especially if the air is moist, allows a complex network of chemical reactions to proceed that normally do not take place. These reactions produce a gas mixture of changing chemical composition which may have different electrical properties than undosed air. In particular it is the conductivity of highly dosed air that is the important parameter in late-time EMP calculations.

One phenomena that may indicate a discrepancy between the actual electric field and that used in EMP calculations is the lightning strokes sometimes seen in the vicinity of a nuclear burst. Based on the conductivity of undosed air, the late-time electric field has been found to be "on the order of but somewhat less than that estimated to be necessary to initiate a discharge." (Ref. 2) It has recently been postulated that highly dosed air may contain enough HNO_3, a highly electronegative species, to increase the electron attachment rate and reduce the conductivity. (Ref. 3)

The work reported here is an integral type of experiment to compare the electron conductivity of highly dosed air at various times after the dose is absorbed to the electron conductivity of undosed air. At the same time the ion current as a function of time was measured. Incidental to the late-time measurement of air conductivity, experimentation was carried out on ionization enhanced breakdown in air. This effect may also be relevant to nuclear "lightning" since breakdown was observed at field strengths very much lower than those necessary to breakdown normal air.

SECTION 2

THEORY OF MEASUREMENT

The conductivity, σ, is defined by the equation

$$\sigma = n\, e\, \mu \tag{1}$$

where n is the number density of the charge carriers and μ is their mobility. Since n for a gas depends upon the waveform of the ionizing radiation as well as the total dose, conductivity is not a basic property of the gas. When electron impact multiplication and sweep-out in the gas can be ignored, the free electron number density is given by

$$n_e(t) = K\, P\, e^{-\alpha t} \int_0^t \dot{D}(t')\, e^{\alpha t'}\, dt' \tag{2}$$

where K is a constant that depends upon the energy needed to produce an electron-ion pair in the particular gas, P is the pressure, α is the electron attachment rate, and $\dot{D}$ is the applied dose rate.

In the case of late-time EMP the dose rate changes slowly compared to the electron attachment time, α^{-1}. There then exists a quasi-steady state and Equation (2) reduces to

$$n_e(t) = \frac{K\, P\, \dot{D}(t)}{\alpha} \tag{3}$$

and the conductivity becomes

$$\sigma_e = KP\dot{D}\, e\, \frac{\mu}{\alpha} \tag{4}$$

Thus it is only necessary to measure the ratio of mobility to attachment rate for highly dosed air to determine the conductivity of interest in late-time EMP.

This measurement was made using the parallel-plate ("pie-pan") ionization chamber shown in Figure 1. The chamber was used in a previous study of the electron conductivity of dry and wet undosed air. (Ref. 4) The double-sided configuration reduces spurious Compton currents and increases the collection area. The high voltage is applied to the center plate and ionizing radiation enters the chamber through the thin aluminum windows. Free charge moving in the applied field between the plates produces a current in the circuit connected between the center and outer, grounded electrodes.

With a plate separation, d, of 1.4 cm and an applied voltage, V, of 600 V, the electron transit time across the gap is $\sim 3\times10^{-6}$ s. Since this is very much larger than the attachment time, sweep-out is small and Equation (2) is applicable. The electron current measured by the chamber is then

$$I(t) = 2\, n_e(t)\, e\, \mu\, E\, A \tag{5}$$

where the factor of 2 arises from the double-sided construction of the ion chamber, E is the applied electric field, and A is the area of the chamber that has been irradiated. The total charge measured by the ion chamber can be obtained by directly integrating Equation (5) with Equation (2) for $n_e(t)$, yielding

$$Q = 2\, K\, P\, D\, e\, E\, A\, \frac{\mu}{\alpha} \tag{6}$$

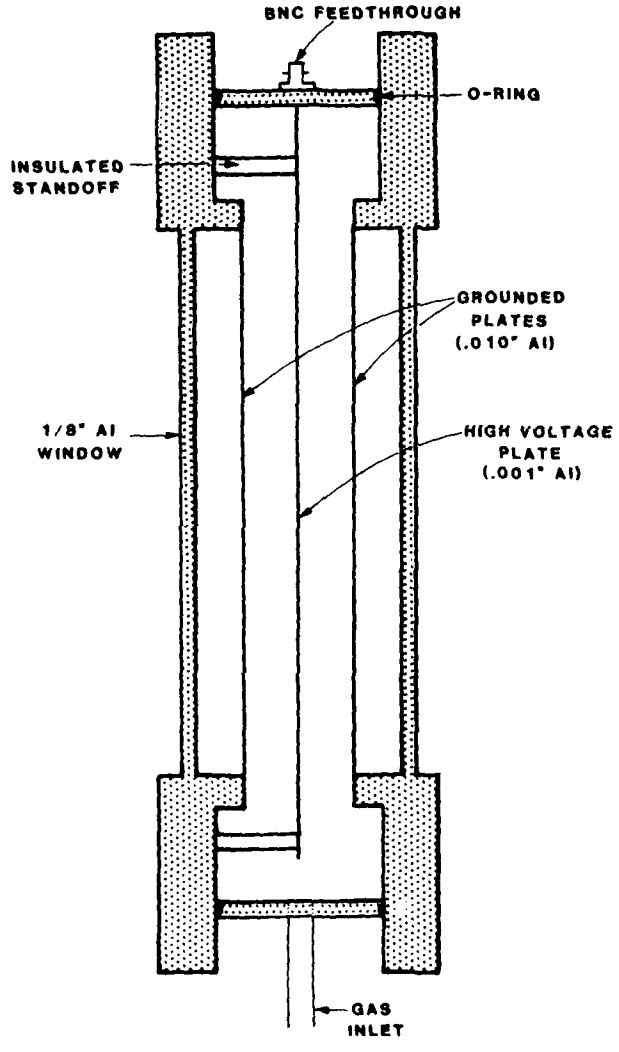

Figure 1. A not-to-scale drawing of the side view of the parallel plate ion chamber.

where D is the total dose. Thus the area under the electron current waveform is a measure of μ/α even when the waveform does not follow the ionization waveform. This is the case in this experiment where the 3 ns wide radiation pulse from the Febetron is smaller than the approximately 10 ns electron attachment rate at atmospheric pressure. The independence of μ/α from the waveform also allowed the use of a transformer with a 50Ω insertion impedance and rise time of 20 ns to measure the electron current.

Equation (1) also applies to the ions produced in a gas. The initial positive ions and the negative ions produced by electron attachment exist in the gas for much longer times than the free electrons. The rate of ion removal is proportional to the square of the ion density, resulting in an ion density as a function of time given by

$$n_i(t) = \frac{n_i(0)}{1 + n_i(0)\beta t} \tag{7}$$

where β is the ion-ion recombination coefficient.

In our ion chamber the ion current is

$$I(t) = 2x2\ n_i(t)\ e\ \mu_i\ E\ A \tag{8}$$

where one factor of 2 is for the two sides and the other factor of 2 is for the two polarities of ions. An average ion mobility for both positive and negative ions, μ_i, is used.

The electric field in Equations (5) and (8) is the electric field seen by the electrons and ions in the bulk of the gas. As the ions drift towards the plates in the applied field a boundary layer is formed at the positive and the negative plate. These boundary layers will screen the bulk of the gas from the applied field. The fraction of the applied voltage that is dropped across the two boundary layers is

$$\frac{\Delta V}{V_o} = \frac{\rho}{\varepsilon_o V_o} x^2 \tag{9}$$

where ρ is the charge density in the boundary layer and x is the thickness of the boundary layer.

If the chemical species created in the highly dosed air can diffuse to the walls while the chemistry is taking place, the reactions and resulting gas mixture can be affected by interactions with the walls. The longest time after the dose that measurements were taken was 10 ms. If we conservatively assume a molecular diffusion coefficient of 1 cm^2/s, the diffusion length is given by

$$\begin{aligned} L &\sim \sqrt{D\ t} \\ &\sim 0.1 \text{ cm} \end{aligned} \tag{10}$$

This is only about 7 percent of the separation distance of the plates, so diffusion to the walls will not serious effect the results of the experiment.

SECTION 3

EXPERIMENTAL

3.1 COLLIMATION AND SHIELDING

In order to simulate the energy deposition from the Mike shot nuclear burst at a distance of approximately 1000 meters (the distance at which the lightning was observed), a dose on the order of 10^6 rad is required. This was obtained from the HERMES II generator operating in the e-beam mode. Figure 2 shows the geometry of the experiment with the ion chamber mounted inside the HERMES II drift chamber. The pressure in the drift chamber was maintained at about 30 torr for e-beam propagation. A new rear plate for the drift chamber was manufactured with electrical feedthroughs for the signal cable to the ion chamber, the connection to the thermistor mounted on the rear of the ion chamber, and for a heat tape (not shown in Figure 2) which could be used to maintain the chamber at an elevated temperature. A gas feedthrough was installed in the rear plate to allow venting and filling of the ion chamber. A 1" thick aluminum (a convenient low Z element) stopping plate was attached to the back plate to prevent the electron beam from penetrating into the room. Since all of the electrons from HERMES II are less than 10 MeV, a thickness of 5 gm/cm^2 will stop all the electrons.

A 1" thick aluminum collimator was mounted on the front of the ion chamber to restrict the region of highly dosed air to the center of the ion chamber while minimizing Bremsstrahlung production. The diameter of the opening in the collimator was 8 inches while the electrodes in the ion chamber were over 10 inches in diameter. A lead collimator 1/8" thick

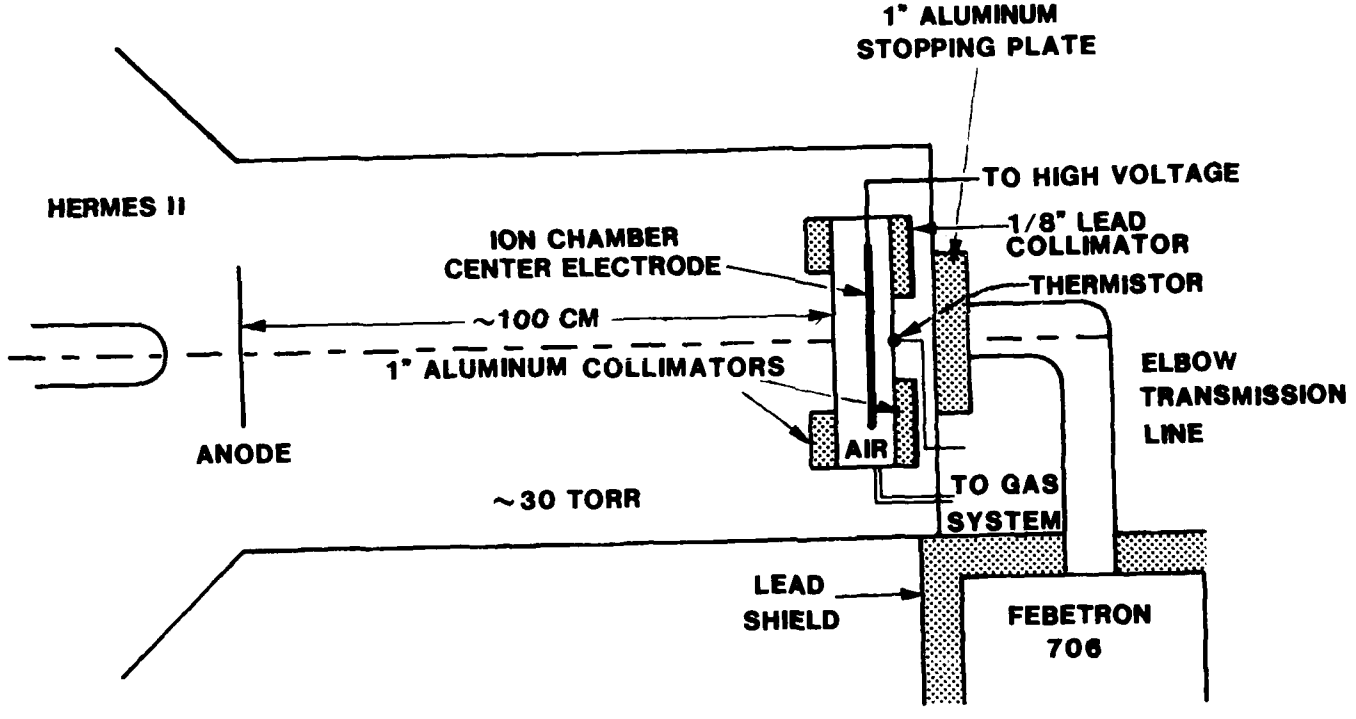

Figure 2. Geometry of experiment. (not to scale)

was used at the rear of the ion chamber to insure that the x-ray beam from the Febetron irradiated only air that had previously received the electron dose. The Febetron was placed as close as possible to the ion chamber to maximize the x-ray dose. Thus, the divergence of the x-ray beam through the ion chamber was quite large. Since the lead collimator would have been illuminated by the electron beam that penetrated the ion chamber, a second 1" thick aluminum collimator was mounted on the rear of the ion chamber to shield the lead collimator from the e-beam.

The highly dosed air is produced by the HERMES II e-beam, and the x-rays from the Febetron 706 reintroduce free electrons into the gas for the measurement of μ/α. The Febetron was removed from the most intense region of radiation produced by HERMES II by the use of a right angle bend in its high-voltage transmission line. Despite the attempts to keep the HERMES II produced Bremsstrahlung to a minimum, about 70 rads were recorded on the case of the Febetron with TLD's. This radiation caused the Febetron to fire immediately whenever HERMES II was fired. After investigation of the amount of radiation needed to prefire the Febetron spark gaps and mapping of the radiation in the HERMES II test cell by Sandia personnel, it was found that 4 to 8" of lead shielding along the front and side of the Febetron case was sufficient to reduce the dose to < 1 rad and prevent the prefiring of the spark gaps.

3.2 E-BEAM PROPAGATION

It is important that the e-beam be fairly uniform across the front of the ion chamber. If the beam were to filament and produce regions of highly dosed air as well as regions of only lightly dosed air, the current from the lightly dosed air would mask any increase in electron attachment in the highly dosed air, making the experiment inconclusive. For example, if one half of the volume of the ion chamber was filled with highly dosed air and one half filled with normal air, a factor of 10

increase in α in the highly dose air would cause only a 45% decrease in the current measured by the ion chamber. Propagation of the e-beam in the drift chamber was studied before installation of the ion chamber with a segmented, graphite, total-beam stopping calorimeter. Initially a graphite collimator with a 4" diameter hole was mounted in the front of the drift chamber. This collimator had been previously used with success when a quartz tube (part of the previous experiment's apparatus) was placed down the axis of the drift chamber. Without the quartz tube, which was operated at pressures in the 20-100 torr range, the beam quickly expanded as it exited the collimator, even at pressures as high as 400 torr. When the collimator was removed high fluence propagation was achieved. At high pressure ($\geq$ 100 torr) the beam had too small of a diameter and at low pressure ($\leq$ 10 torr) the beam expanded too quickly. At intermediate pressures a uniform beam of about the correct fluence was propagated down the drift chamber.

The calorimeter was mounted in the chamber $\sim$ 100 cm from the anode, approximately at the position of the front face of the chamber during the experiment. An aluminum plate with an $\sim$ 8" aperature was mounted at the front surface of the collimator and grounded to the drift chamber to simulate the distribution of conducting surfaces during the actual experiment. The total energy absorbed in the calorimeter as a function of pressure is shown in Figure 3a. The spatial distribution of the fluence over the surface of the calorimeter at the chosen pressure of 30 torr is shown in Figure 3b. (Ref. 5) The largest ratio of the fluence in one segment to that in another is 2.3, but the ratio of fluence in the inner ring of segments to the fluence in the outer ring of segments is 1.1. The diameter of calorimeter was approximately 4" while the opening in the ion chamber collimator was 8". The uniformity of the beam over the larger area was checked on one shot during the experiment using a radiation sensitive plastic, cinemoid. The ratio of the dose at the center of the ion chamber window to that at a radius of 4" was 2.1. During the calorimetry study a

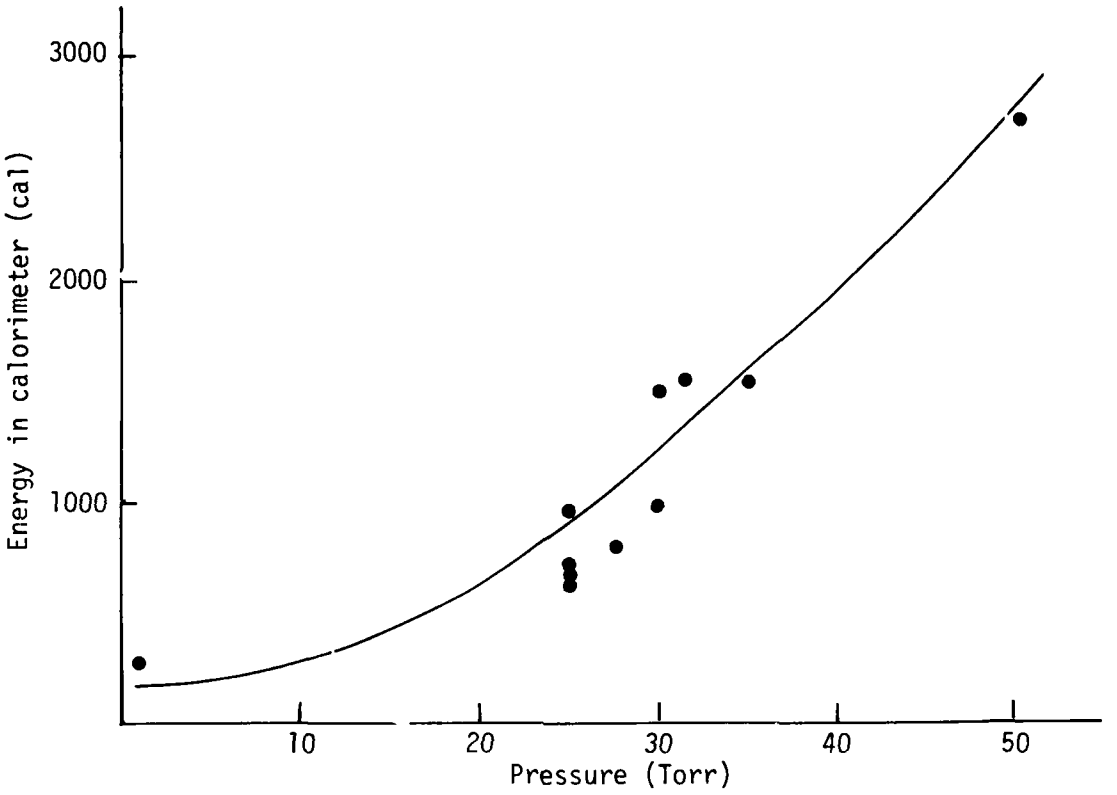

a) Total energy into calorimeter versus pressure.

	11.9	14.6	14.5	
8.6	11.8	12.1	14.4	12
8.3	8.1	12.5	12.7	11.5
6.2		9.4	10.8	10
		10.2	9.2	

b. Fluence distribution across calorimeter (cal/cm^2) on a shot at 30 torr.

Figure 3. E-beam calorimetry.

camera was set up to photograph the air luminescence through a window in the drift chamber. No filamentation of the beam was observed at the 30 torr operating pressure.

During the experiment the calorimeter was removed and a thermistor was used to measure the temperature increase of the ion chamber on HERMES II shots. The thermistor was held in electrical and thermal contact with the rear window of the ion chamber by taping a piece of spongy material over it. (This avoided a previously encountered problem of the thermistor being loosened by thermal shock when the thermistor was epoxyed to the chamber.) The thermal relaxation constant of the chamber window was estimated to be greater than 10 s and in fact was measured to be greater than 1 min as shown by the thermistor output on a HERMES II shot in Figure 4. The dose was calculated from the temperature rise and the published curve of $(cal/gm)/(cal/cm^2)$ for the HERMES II spectrum (Ref. 6) The HERMES II dose did not enter into the calculation of any quantities found in this experiment; it is only necessary to insure that highly dosed air is being made in the ion chamber.

3.3 EXPERIMENTAL SEQUENCE

The experiment proceeded according to the following sequence of events:

(1) A ~ 100 ns pulse of ~ 8 MeV electrons from HERMES II delivered a dose of ~ 2×10^6 rad to the air in the ion chamber.

(2) After a variable waiting time (0.2 to 10 ms) for the chemical reactions to proceed, 600 volts were applied to the plate of the chamber.

(3) Ninety (90) μs later, the ion current was measured.

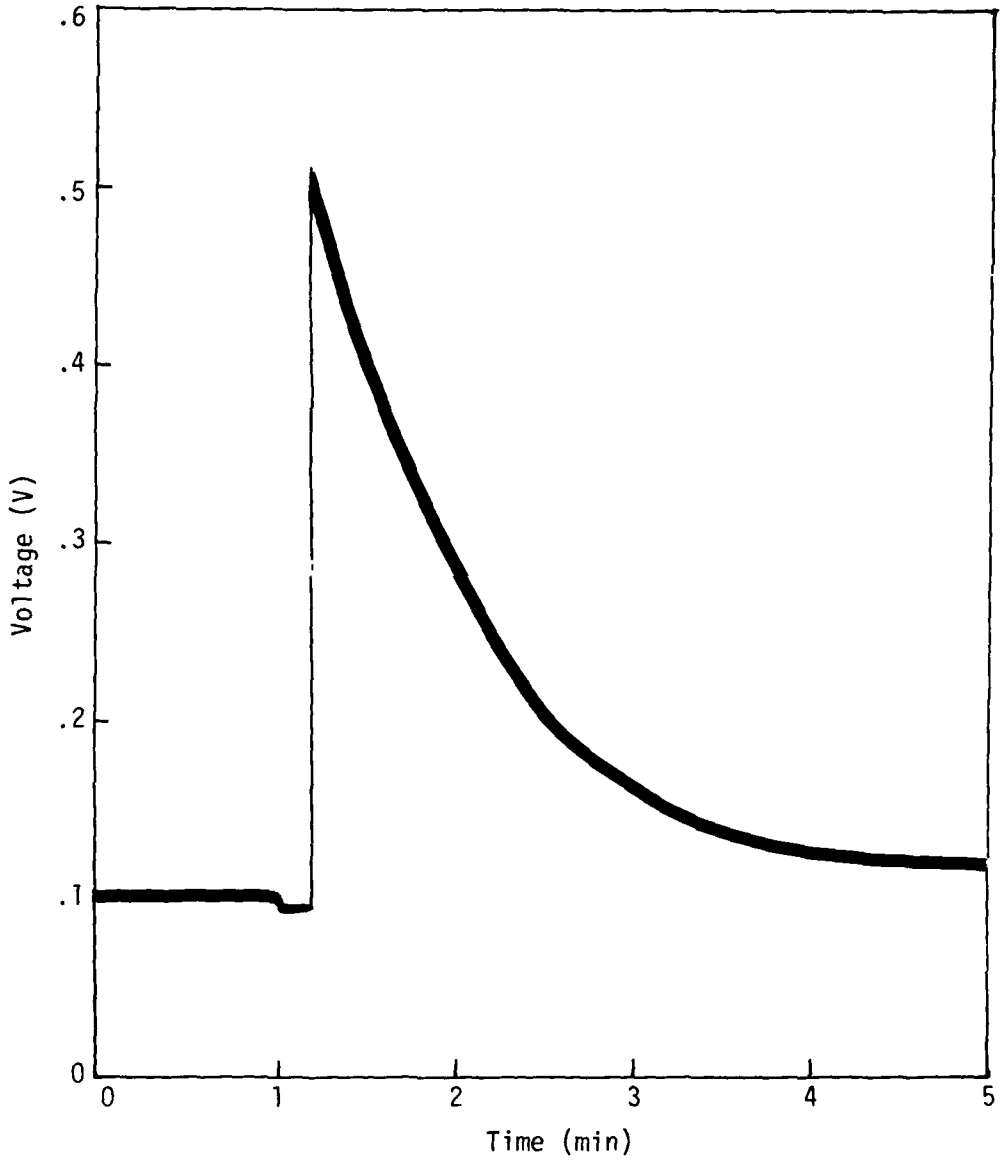

Figure 4. Thermistor output on HERMES II shot #H690

(4) After another 50 μs wait (or simultaneously in some cases), the Febetron was fired delivering ~ 50 mrad to the air in the chamber and the transient electron current as well as the additional ion current was measured.

During the waiting time (2) the free electrons quickly attach to form negative ions. Positive and negative ions recombine, but because of the form of Equation (6) (for $t >> 1/n_i(0)\beta$, $n(t) = 1/\beta t$) a significant number of ions remain at the end of the waiting period. It is important to apply the electric field quickly to the plates and to make the ion and electron current measurements soon after the field is applied because the drift of the ions will be establishing the boundary layers during this time. The 90 μs used here was a compromise between the desire for a quick measurement and the limitation of the electronics. Actually 50 μs was a 10 time constant wait for the charging of the plates and 40 μs was needed for the amplifier used to measure the ion current to settle down after the inputs were unclamped from ground. The additional 50 μs delay before firing the Febetron separates the ion current due to the initial HERMES II ionization from that due to the firing of the Febetron.

The importance of the boundary layer can be estimated from Equation (9) which for this experiment takes the form

$$\frac{\Delta V}{V} = \frac{e\, V\, n_i(t)}{\varepsilon_0} \left(\frac{\mu_i\, t'}{d}\right)^2 \qquad (11)$$

where t is the time from the firing of HERMES II to application of the field, and t' is the time from application of the field to the measurement of ion or electron current. Equation (11) gives somewhat of an overestimate because it assumes that the whole voltage is applied during the charging time. For a waiting time of 1 ms we measured a remaining ion density of $\sim 10^9$ cm^{-3}. For measurement of the electron current t' = 90 + 50 = 140 μs, and assuming μ_i = 2.0 cm^2/V-s, Equation (11) yields

$\Delta V/V = 0.04$. At 1 ms the measurement is affected by 4 percent or less due to the boundary layer while at 0.2 ms, where there are roughly five times as many ions remaining, about one fifth of the applied voltage will be dropped across the boundary layer.

3.4 ELECTRONICS

The circuit used to produce the desired timing and to measure the ion and electron currents is shown in simplified form in Figure 5. The high-voltage power supply charges the 1 μF capacitor which then charges the plate of the ion chamber when transistorized switch S1 is closed. S2 is closed when S1 is open to provide a path to ground for the leakage current through the transistor of S1. When the voltage is applied, S2 is opened. The transient electron current flows from the center plate of the ion chamber through the 0.001 μF capacitor to ground and is measured through a 1:1 pulse transformer terminated in 50Ω at the scope or 7912 transient digitizer. A CT-1 current probe (not shown) with a smaller insertion impedance and smaller transfer impedance was also used to measure the electron current. The slower ion current flows through the 1K resistors back to the power supply. Switches S3 and S4 are closed while the ion chamber is being charged to protect the amplifier. Fifty (50) μs after S1 closes, S4 opens and after another 40 μs delay S3 is opened, and the voltage across the 1K measuring resistor is measured with the capactively coupled instrumentation amplifier.

The timing circuit used to operate the switches was located in the instrumentation van; the high-voltage power supply, switches, and amplifier were placed behind a concrete wall in a fairly low radiation environment approximately 30 ft from the ion chamber; the electron current transformer and 0.001 μF capacitor to ground were located as close as possible to the ion chamber at the rear of the drift chamber in order to minimize cable capacitance. The positioning of the amplifier and switches

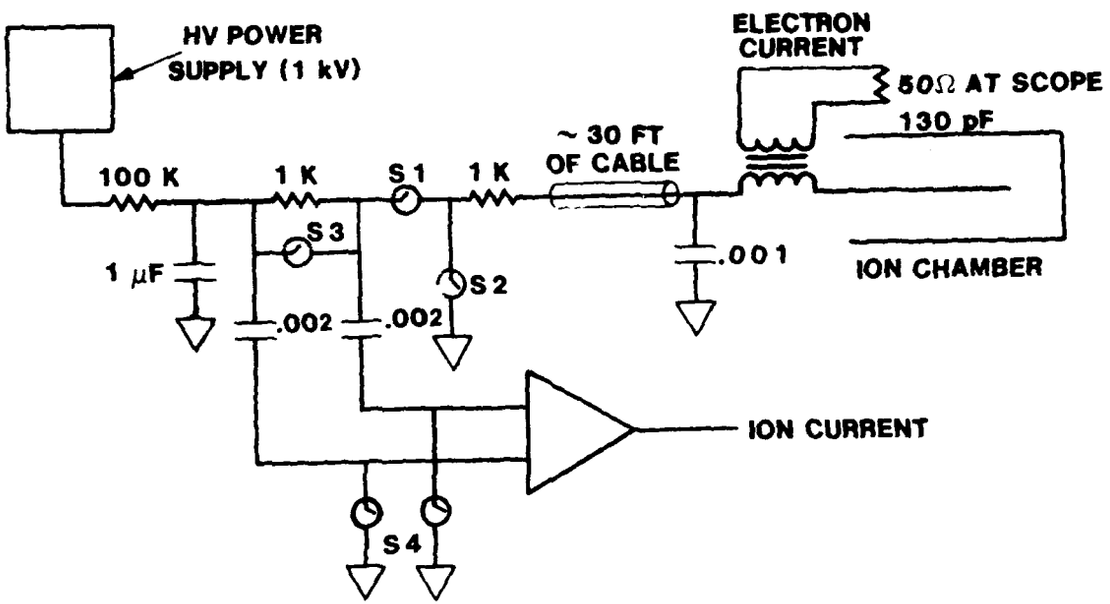

Figure 5. Simplified circuit diagram.

was a compromise between the desire to charge the ion chamber quickly and thus to keep the cable capacitance between the switches and chamber small, and the avoid firing of the switches by the HERMES II radiation. The electrical connections from the HERMES test cell to the instrumentation van and behind the wall are shown in Figure 6.

In order to avoid ground loops the Febetron was grounded only through its connection to the Febetron control console which was in turn grounded at its power cord. Thus, it was necessary to use pulse transformers in the line to the Febetron voltage monitor and the trigger line to the Febetron control console as shown in Figure 6. The TRANS, CT1, and ION signals were recorded on both oscilloscopes and 7912's. The TRANS and CT1 signals were triggered by the Febetron voltage monitor and ION signal by a timing signal generated in our timing circuit. Counters were used to record the time between the firing of HERMES II and the start of the charging of the plates of the ion chamber and the time between firing of HERMES II and the firing of the Febetron. The timing signals to operate the switches located behind the wall were routed from the VAN via RG22 cable. The thermistor output was monitored during and ~ 10 min after each HERMES II shot on a strip chart recorder.

A timing diagram of the signals generated by the timing circuit is shown in Figure 7. The HERMES trigger is an input signal derived from a PIN diode when HERMES is fired. The switches are reset manually and then switched by the timing signals generated using 555 IC's. The signal to fire the Febetron is sent out at the same time that switch S3 is opened but it could be delayed by a delay generator integral to the Febetron control console. A detailed schematic of the timing circuit is shown in Figure 8a and b.

Figure 9 is a detailed schematic of the amplifier and switching circuit. Switches S1 and S2 consists of a high voltage, high current

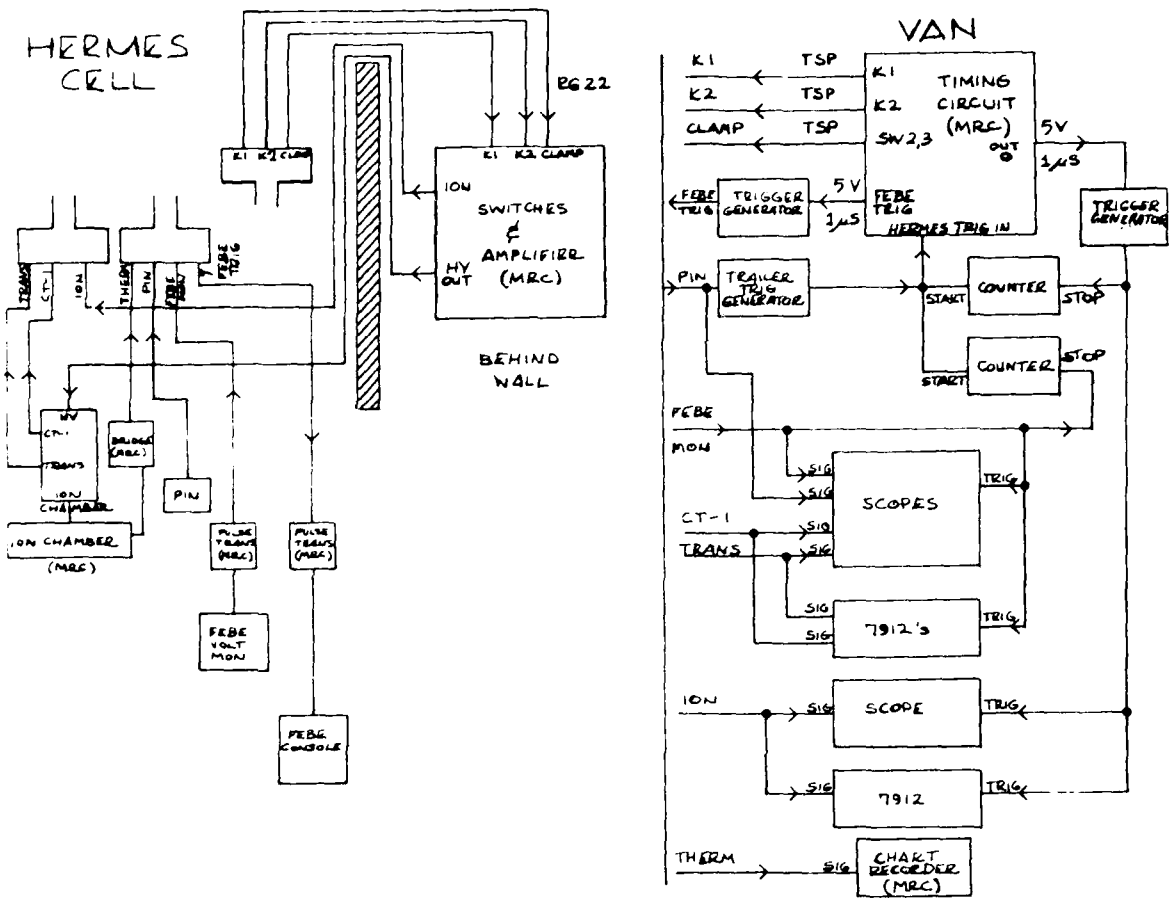

Figure 6. Cable routing diagram.

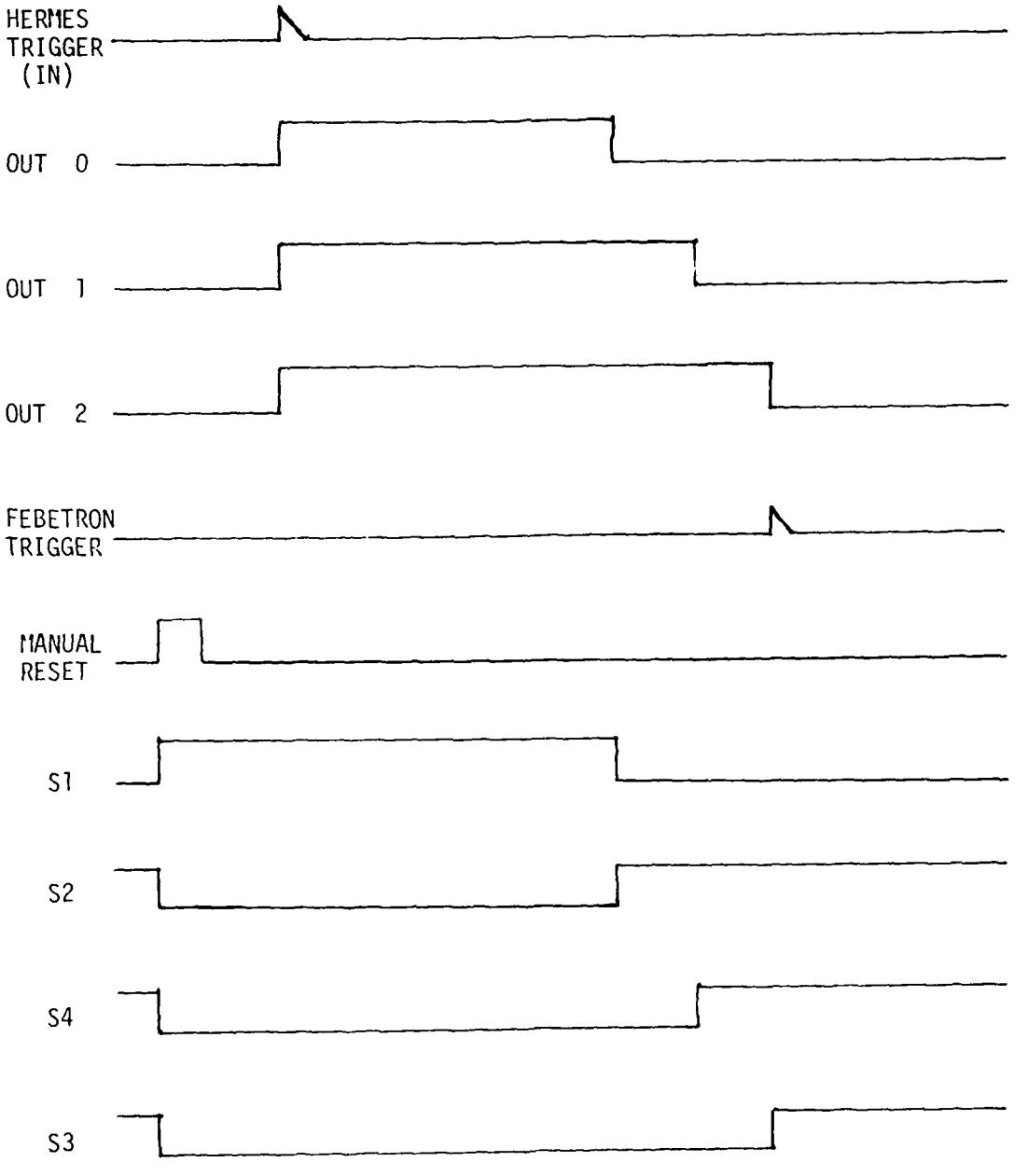

Figure 7. Timing diagram. A high level for a switch indicates that the switch is open.

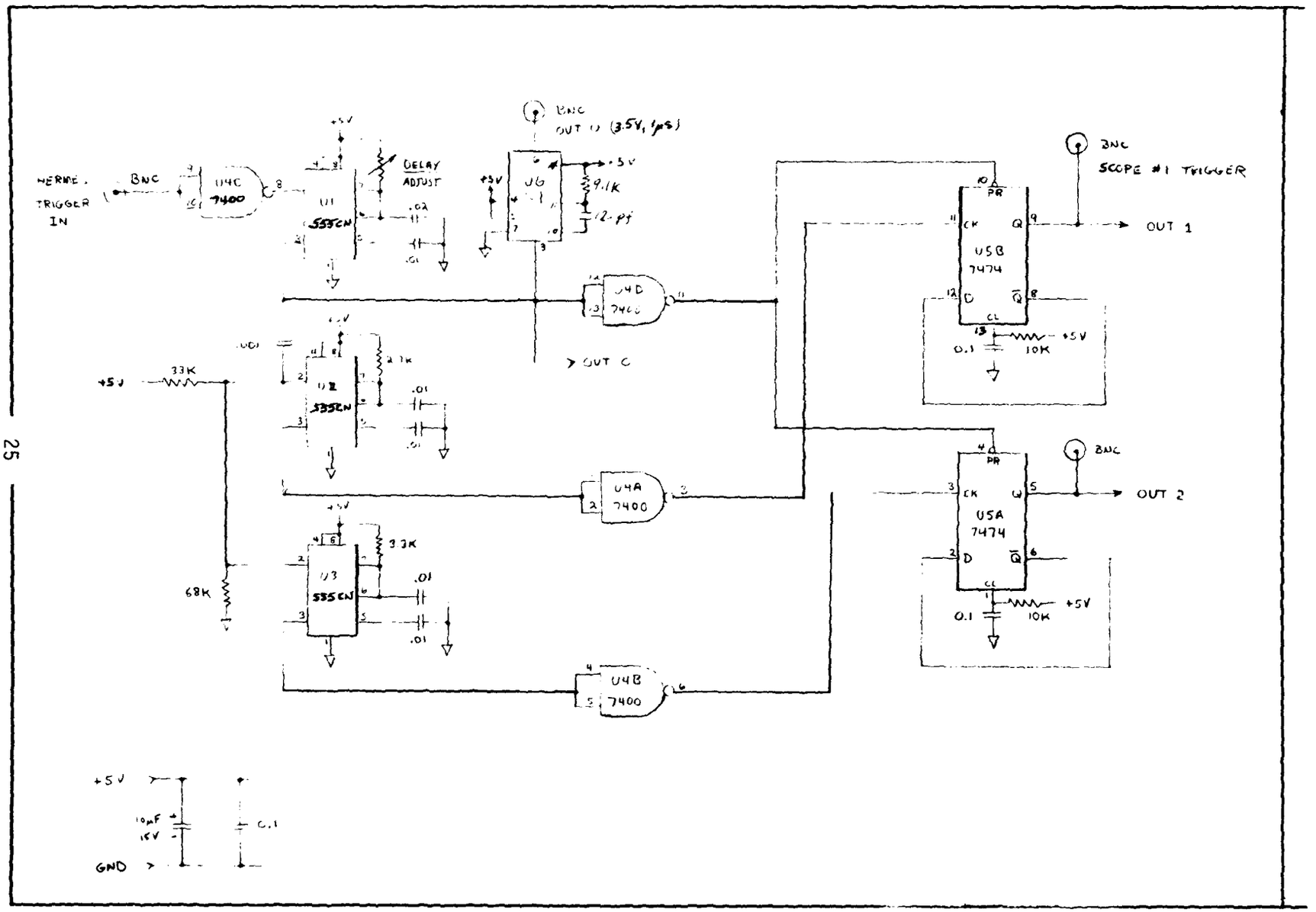

Figure 8a. Timing circuit.

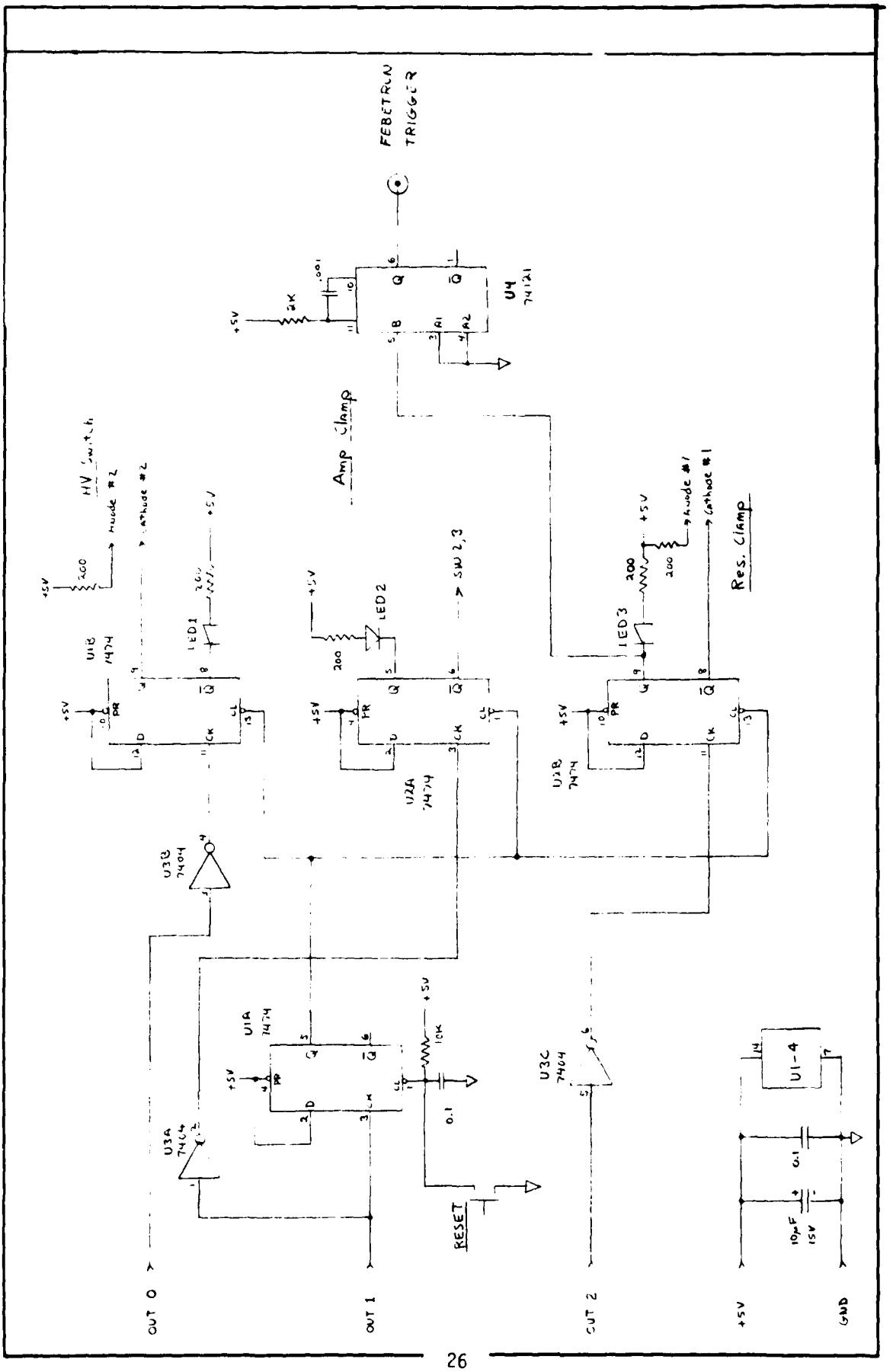

Figure 8b. Switch control circuit.

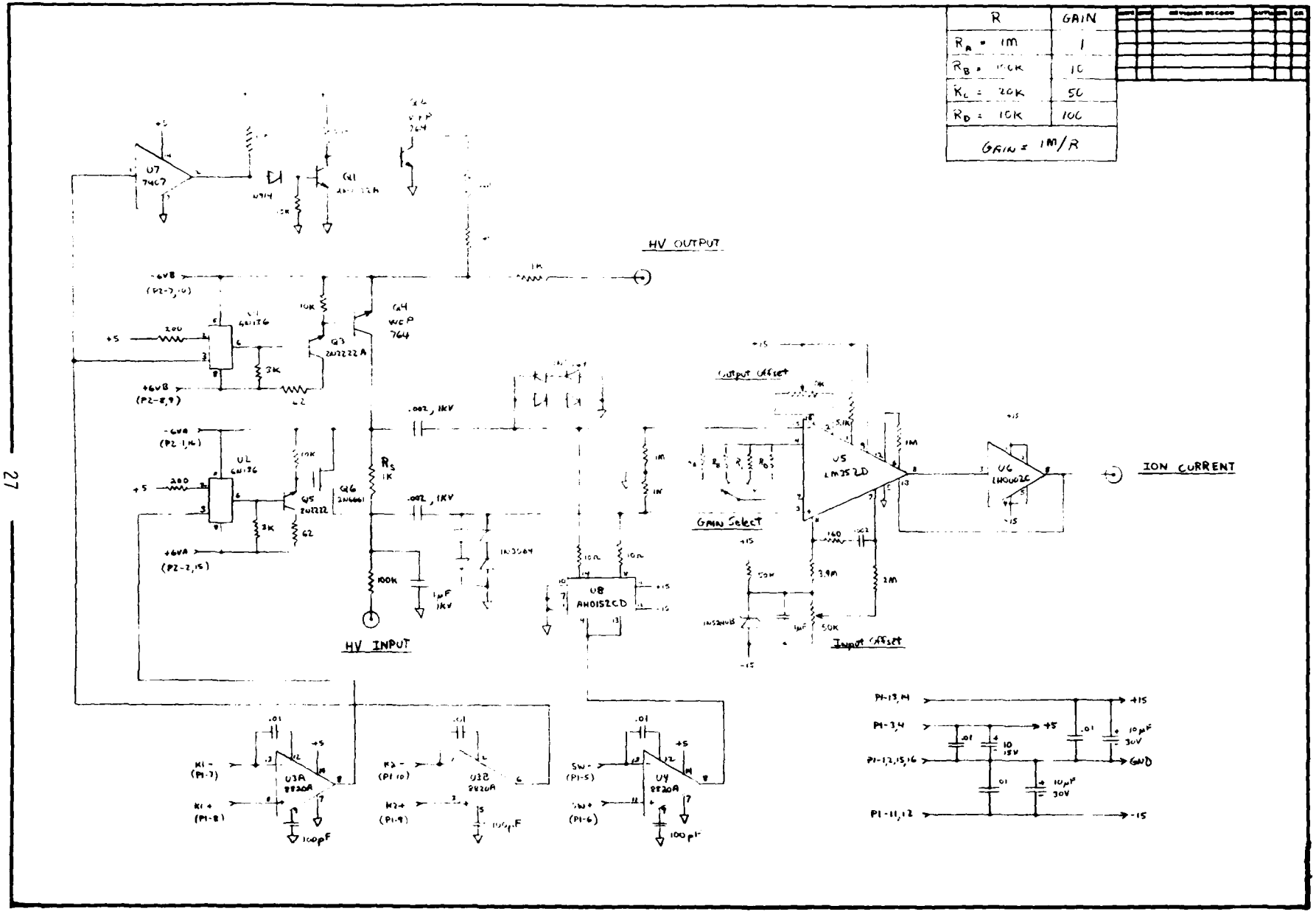

Figure 9. Switching and amplifier circuit.

transistor (WEP 764) driven by a 2N2222 transistor as a darlington pair. Switches S1 and S3 are isolated from the high voltage with optical isolators, 6N136. Switch S4, which clamps both inputs of the instrumentation amplifier to ground until after the large charging current is over and the ion current is to be measured, consists of a AH0152CD analog switch. The gain of the LM352A amplifier was switch selectable between 1 and 100. Differential line drivers were used to drive the ~ 300 ft. of cable separating the time circuits from the switches.

The operation of the switching circuit and amplifier is shown in the waveform of Figure 10a. The ION output is shown with a gain of 100, a charging voltage of 100V, and a load consisting of ~ 30 ft. of cable and a .001 μF capacitor to ground but without the ion chamber connected. The initial downward transient and decay back to the baseline is the large charging current occuring when S1 is closed. It is seen by the amplifier despite the large attenuation due to the shunt switch S3 and ground clamps S4. Approximately 50 μs after S1 closes, the amplifier is unclamped and the output assumes the output offset voltage of the amplifier. (This offset voltage could be adjusted to zero if desired.) After 40 μs, the shunt across the measuring resistor was opened and after a switching transient the output assumes a voltage proportional to the leakage current through the load. Figure 10b is for identical condition as Figure 10a except that a 100 MΩ resistor to ground has been added to the load. Comparison of Figure 10a and b show that the 1 μA current through the load resistor is easily measured.

The measurement of the transient electron current with the CT-1 and transformer was hindered by a large voltage (~ 2V for 2 ms) presumably due to a ground loop current. In an effort to reduce ground currents on the shields of our signal cables, the Febetron was isolated from HERMES and the instrumentation van. The electronics located behind the wall was floated at the power cord and grounded to the van and drift chamber. The

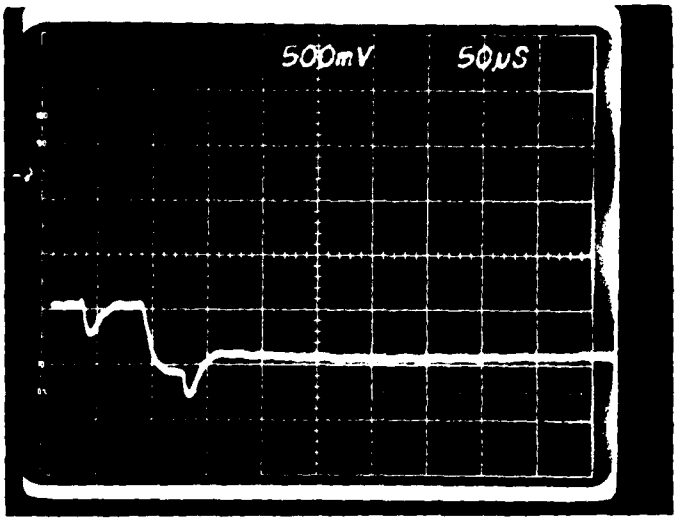

a) Load = cable + .001 μF.

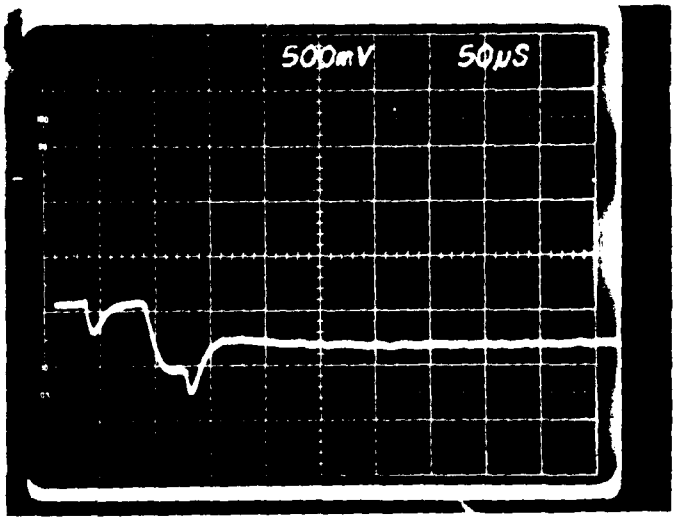

b) Load = cable + .001 μF + 100 MΩ.

Figure 10. Amplifier output. Gain = 100, Charging voltage = 100V.

HERMES voltage monitor, which is normally used to trigger the instrumentation van, consists of a resistor network separating HERMES from the drift chamber. When HERMES was fired a temporary potential difference of ~ 3000 volts is developed between the drift chamber and HERMES ground. The instrumentation van ground was connected to the drift chamber and thus it would rise ~ 3000 V above the HERMES ground. The voltage monitor was disconnected and the resistor string shorted with copper tape. This alleviated a problem with spurious trigger signals that were being generated in the van, but the 2 V for 2 ms noise signal persisted. Thus a high-pass filter with RC = 1 μs was installed in the CT-1 and transformer lines.

3.5 FEBETRON DOSE

The Febetron dose is not needed in this experiment to compare the value of μ/α for highly dosed air to μ/α for undosed air. The dose from the Febetron is of interest as a cross check on the electron and ion currents. The x-ray dose was measured at the front and rear faces of the ion chamber using TLD's and is shown in Figure 11 (Ref. 7). If one assumes that the x-rays have an "average" energy of 100 keV (which is consistent with other attenuation data taken with this Febetron), the attenuation through the aluminum of the chambers is .82. The geometric attenuation between front and back of the chamber is .56. The on axis dose of 153 mrad is expected to fall to 70 mrad in excellent agreement with the 67 mrad measured on the rear face. However, the dose on the front face is constant over a 2" diameter while on the rear face the dose is seen to fall off by almost a factor of 3. The ratio of the dose x area product on the front face to that on the back is found to be 5.7 while attenuation accounts only for a factor of 1.2.

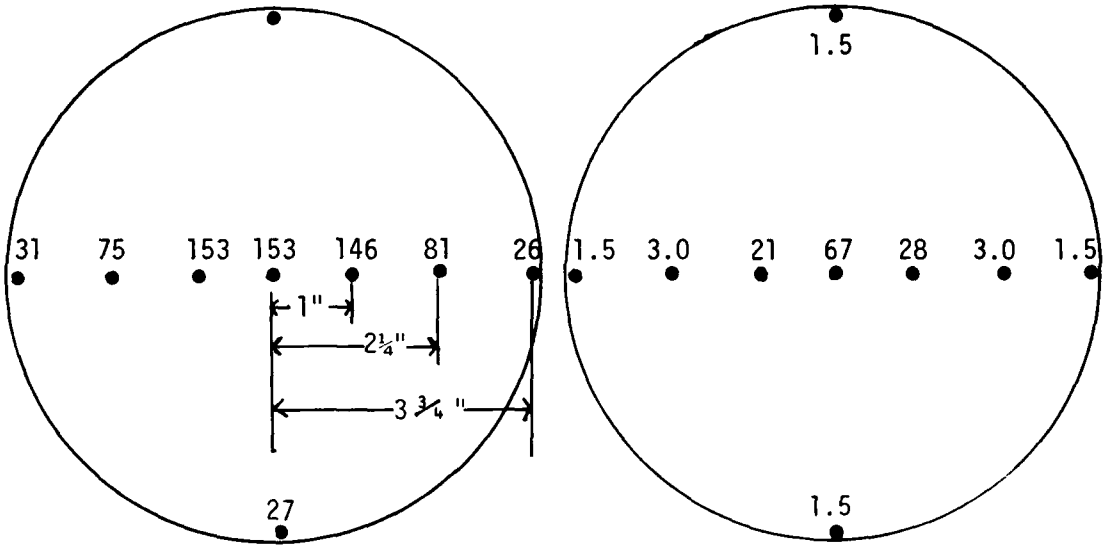

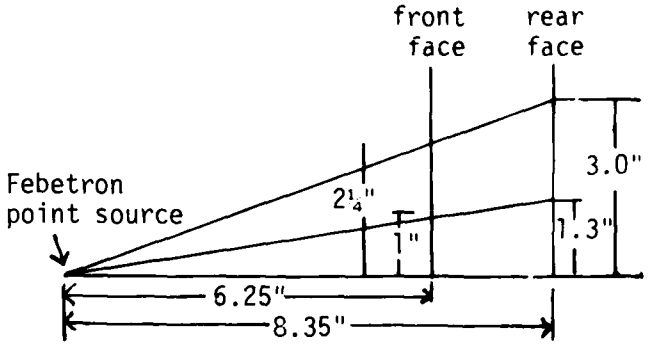

Figure 11. Febetron dose to ion chamber in mrad as measured by TLD's.

The reasons for this discrepancy is not known. The dose x area product can also be calculated from the μ/α values previously measured for wet and dry air (Ref. 8) in conjunction with the electron currents reported in the following section. For the dry air measurements DA = 1.4×10^4 mrad·cm^2 and for wet air DA = 1.2×10^4 mrad·cm^2. Another independent measurement of DA comes from the ion current produced by the Febetron. The values reported in the next section give DA = 1.6×10^4 mrad·cm^2 for dry air and 1.8×10^4 mrad·cm^2 for wet air.

The discrepancy in the values of DA calculated by various methods implies an approximately 40 percent uncertainty in the absolute dose from the Febetron. It should be stressed that this uncertainty in the absolute dose in no way affects the conclusion concerning the comparison of μ/α in highly dosed and undosed air. It is only the relative, shot-to-shot, change in the dose that affects this comparison. The Febetron output was monitored with a PIN detector and shows a shot-to-shot variation of less than 10 percent. Also the uncertainty in the absolute Febetron dose does not affect the ion densities or ion-ion recombination coefficient found below.

3.6 WATER VAPOR CONCENTRATION

Pre-experiment testing of the ion chamber showed that significant amounts of water vapor could adsorb to the aluminum walls of the chamber reducing the water vapor concentration in the air. To avoid this problem, the ion chamber was operated with air satured with water vapor. The temperature of the ion chamber mounted inside the drift chamber as measured by the thermistor was 29.4°C at the time the water was injected into the system. However, the gasline to the chamber was at the room temperature measured with a thermometer to be 25°C. The vapor pressure of the water in the system will correspond to the vapor pressure at the coldest point in the system. At 25°C the vapor pressure of water is 23.7 torr. The

vapor pressure measured with a mercury manometer was 22.5 torr. The chamber was then filled with air to a total pressure of 741 torr giving a water concentration of 3.0 percent.

SECTION 4

RESULTS

A summary of the HERMES II shots and experimental parameters for shots on which data was acquired is shown in Table 1. The dose delivered to the air in the ion chamber by the electron beam when the drift chamber pressure was 30 torr was $2.2\pm.4\times10^{6}$ rad. When the drift chamber pressure was changed to 27 torr the increased divergence of the beam was sufficient to cause the Febetron to be prefired by stray radiation. Although electron current measurement was precluded on prefired shots, ion current was measured on shot H688.

4.1 ELECTRON CURRENT

The results of the electron current measurements are shown in Table 2. In order to make a direct comparison between the conductivity of highly dosed and normal air, the experiment was carried out by measuring the electron current for a series of three shots: Febetron only (B-prefix), HERMES II plus Febetron (H-prefix), and Febetron only (A-prefix). The time between each shot in a series was limited by the time needed to turn around the scopes and 7912's and averaged about five minutes.

The electron current data measured using the transformer were of much higher quality than from the CT-1 because of the larger signal amplitude and because of excessive noise on the CT-1 cable which could not be easily suppressed. Only the data from the transformer are reported here. The current waveform from the transformer was recorded on both a scope and a 7912. A typical scope waveform (after smoothing and digitizing) is

Table 1. HERMES shots on which data was taken.

SHOT NUMBER	DATE	DRIFT CHAMBER PRESSURE (torr)	DOSE (Mrad)	DELAY (ms)	CHAMBER VOLTAGE (V)	ION CHAMBER CONTENTS
H686	02/21/80	30	2.9*	1.0	600	1 atm dry air
H687	02/21/80	30	2.1	10.1	600	1 atm dry air
H688	02/22/80	27	Cable not connected	Febetron pre-fired	600	1 atm dry air
H689	02/22/80	27	0.9	Febetron pre-fired	600	1 atm dry air
H690	02/22/80	30	2.3	1.2	600	1 atm dry air
H691	02/22/80	30	2.2	1.2	600	1 atm air, 3% H_2O
H692	02/22/80	30	1.6	9.8	600	1 atm air, 3% H_2O
H693	02/22/80	30	2.2	0.2	600	1 atm air, 3% H_2O
H694	02/22/80	30	HERMES MALFUNCTIONED			

*By cinemoid; the rest by thermistor measurement of ion chamber temperature.

Table 2. Charge measured from Febetron shots in Highly dosed and undosed air.

SHOT NUMBER	DELAY (ms)	CHARGE (nC)		COMPARISON (STANDARD DEVIATIONS)	GAS
		SCOPE	7912		
B686	1.01	0.104		-1.2	1 atm dry air
H686		0.109			1 atm dry air
A686		0.118	0.131		1 atm dry air
B687	10.10			+1.9	1 atm dry air
H687		0.153			1 atm dry air
A687		0.106			1 atm dry air
B688	Febetron pre-fired	0.151	0.129		1 atm dry air
H688					1 atm dry air
H689	Febetron pre-fired				1 atm dry air
B690	1.15	0.122	0.136	+0.6	1 atm dry air
H690		0.135			1 atm dry air
A690		0.139	0.121		1 atm dry air
B691	1.19		0.079	+0.2	1 atm air + 3% H_2O
H691		0.076			1 atm air + 3% H_2O
A691		0.070	0.063		1 atm air + 3% H_2O
B692	9.80	0.057	0.058	-1.1	1 atm air + 3% H_2O
H692		0.060			1 atm air + 3% H_2O
A692		0.088	0.062		1 atm air + 3% H_2O
B693	0.20	0.086	0.078	-0.5	1 atm air + 3% H_2O
H693		0.067			1 atm air + 3% H_2O
A693		0.096	0.083		1 atm air + 3% H_2O

shown in Figure 12; the charge found from integrating the area under the curves is listed in Table 2. Although the interesting chemistry was expected to take place in wet air, dry air was studied first both as a check on the wet air results and to determine the Febetron dose from the dry air electron current.

Since the after (A-prefix) shots occurred so long after the HERMES II shot, it is expected that the air will have returned to its normal, undosed state. This is verified by comparing the average charge on before shots to that on after shots. These average values fall within 0.3 standard deviations of each other for both dry and wet air. Lumping the before and after shots together, we find for dry air an average charge of $0.125 \pm .015$ nC and for wet air an average charge of $0.074 \pm .013$ nC. These values for undosed air are compared to the charge measured in highly dosed air in column 5 of Table 2. Here is listed the number of standard deviations by which the charge measured on HERMES II shots differed from the average value on Febetron-only shots. We see that for all measurements in highly dosed air the charge, and thus μ/ω, for highly dosed air falls within two standard deviations of the value for undosed air.

4.2 ION CURRENT

The lifetime of the ions is much longer than the electrons, but because of the much lower mobility, the magnitude of the ion current is much less than that of the transient electron current. The ion current was measured by sensing the voltage across a 1 KΩ precision resistor with an instrumentation amplifier. The output of the amplifier was recorded on a scope and a 7912. A typical 7912 record is shown in Figure 13. The sweep starts as the ion chamber plates are being charged and the trace is off scale. The first, downward step (at 60 ns) occurs when the amplifier inputs are unclamped from ground. The second step occurs when the shunt across the measuring resistor is removed, giving a measure of the ion

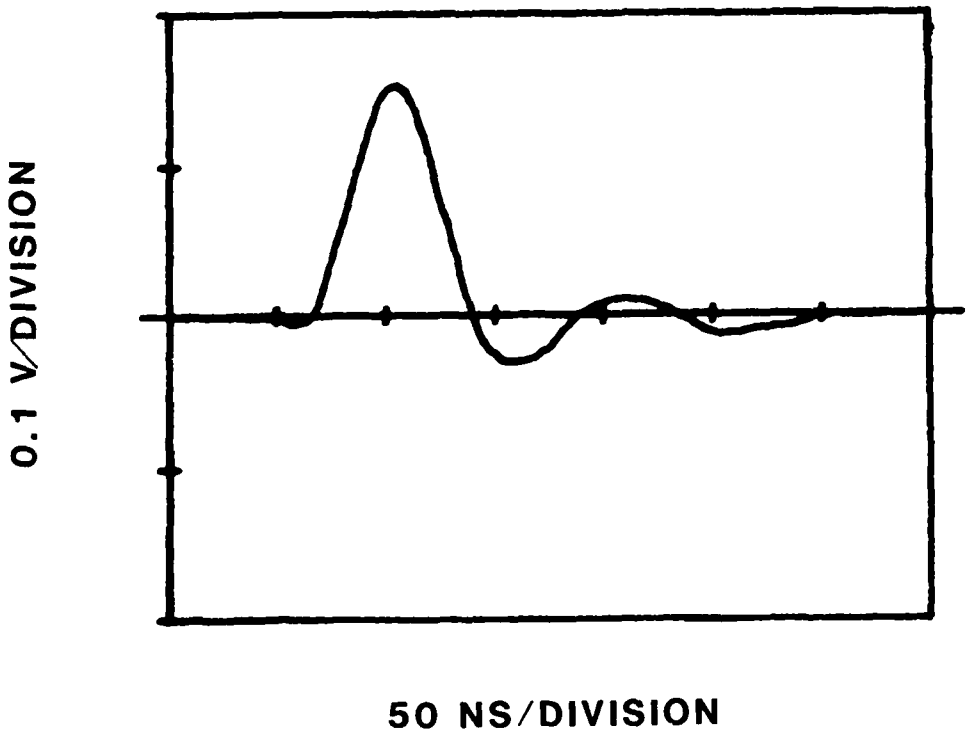

Figure 12. Typical electron current from the transformer.

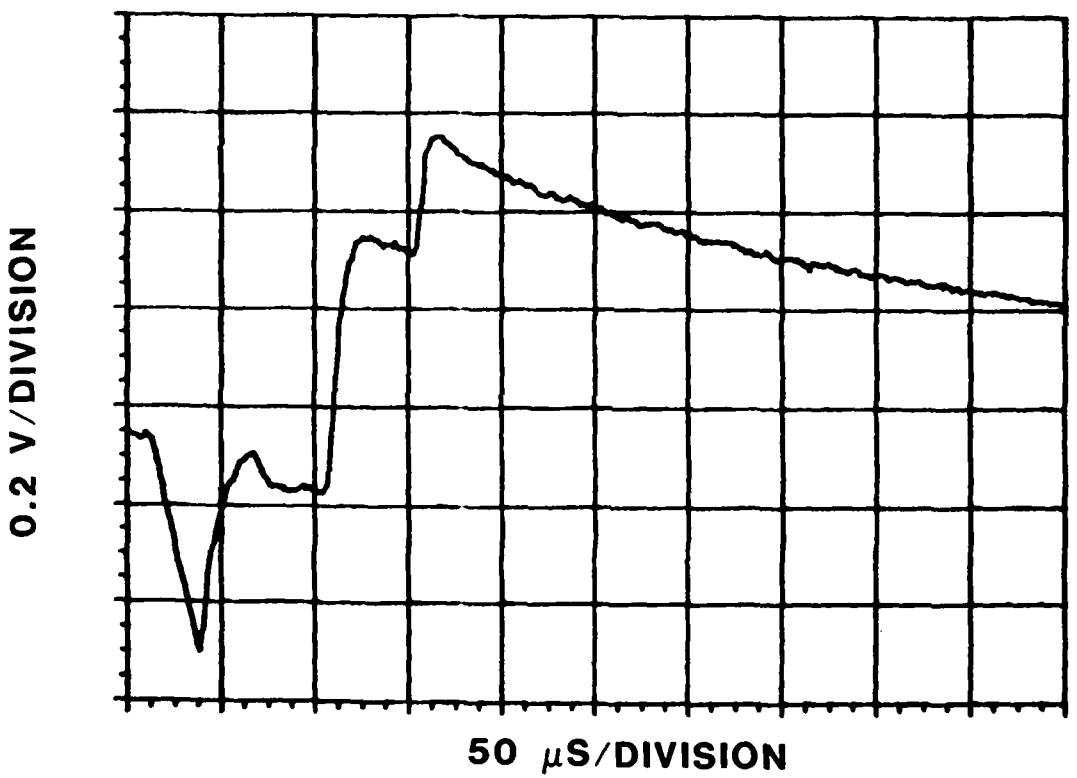

Figure 13. Ion current on HERMES II plus Febetron shot.

current remaining from the HERMES II dose. The third step occurs when the Febetron is fired and additional ions are created in the air. If neither HERMES II nor the Febetron are fired there will still be an upward step when the shunt is removed due to leakage current in the cable, chamber, 0.001 μF capacitor, and switch S2. This offset current which was recorded several times during the experiment must be subtracted from the current recorded in Figure 13 to get the ion current.

Table 3 shows the measured ion currents from the Febetron and at various times after a HERMES II pulse. The initial Febetron ion current is quite constant at a value of 18.2±1.3 μA for dry air and 17.5±1.7 for wet air. This statistical variation of about 10 percent is due to pulse-to-pulse Febetron dose variation and measurement precision.

Equation (8) for the ion current can be rearranged to give

$$n_i(t)\ \mu_i = I(t)/4\ e\ E\ A \qquad (12)$$

At late times the ion density given by Equation (7) takes the form

$$n_i(t) = 1/\beta t \qquad (13)$$

The Values of I(t) given in Table 3 can be used in Equation (12) to calculate $n_i\mu_i$, as a function of time to check the time dependency given in Equation (13).

The area to be used in Equation (12) consists of the total area of the ion chamber plates (Ref. 9). This is because Equation (13) shows that the number of ions at late times does not depend upon the initial number of ions created. Even the shielded volume of the chamber receives enough of a dose that the ion concentration is uniform throughout the chamber at the time of the current measurement. The gap width changes

Table 3. Ion current from remaining HERMES II ionization and from Febetron dose.

SHOT NUMBER	DELAY (ms)	ION CURRENT (μA)				OFFSET CURRENT (μA)		GAS
		FEBETRON		HERMES II		SCOPE	7912	
		SCOPE	7912	SCOPE	7912			
B686 H686 A686	1.01	18 16	18 18			5.2		1 atm dry air
B687 H687 A687	10.10	20 18		29	30	5.9	5.6	1 atm dry air
B688 H688	0.70			480				1 atm dry air
B691 H691 A691	1.19		 19	320	290			1 atm air + 3% H_2O
B692 H692 A692	9.80	16 16 19	 16 19	36	36	6.5 7.1	 7.6	1 atm air + 3% H_2O
B693 H693 A693	0.20			910	860			1 atm air + 3% H_2O

abruptly from 1.4 cm to 2.6 cm so there are two collecting regions with different electric fields and having areas of 616 and 374 cm^2 respectively. Equation (12) becomes

$$n_i(t)\ \mu_i = I(t)/4\ e\ (E_1\ A_1 + E_2\ A_2) \qquad (14)$$

Figure 14 shows the measured product of ion density and mobility as a function of time. The data point at 0.2 ms is expected to be low because of the development of a boundary layer. The other four data points fall along a straight line with a slope of -1, indicating that the data is described by Equation (13). From the straight line in Figure 14 the ratio μ_i/β is found to be 1.6×10^6 $cm^{-1} \cdot V^{-1}$. This value is for 1 atm pressure and a temperature of $\sim 50°C$.

For the pressures used in this experiment, 1 and 0.27 atm, ion-ion recombination is dominated by a three-body, neutral-molecule-stabilized process. This mechanism, called Thomson recombination, is represented by the reaction

$$X^+ + Y^- + M \rightarrow X + Y + M\ . \qquad (15)$$

This reaction proceeds with a rate constant k (cm^6/s). The ion-ion recombination coefficient, β (cm^3/s), is a function of k and the neutral gas density. Sayers has measured β as a function of pressure and found agreement with the functional form of Thomson's theory. (Ref. 10) At 1 atm of air Sayers measures $\beta = 2.2 \times 10^{-6}$ cm^3/s.

The mobility of the "air ions" is needed to compare to our measurement of μ/β. The experimental measurement of ionic mobilities has been complicated because the measured mobility depends on the age of the ions and the identity of the ions formed. Ionic cluster formation and charge exchange to impurity molecules can change the mobility. Although

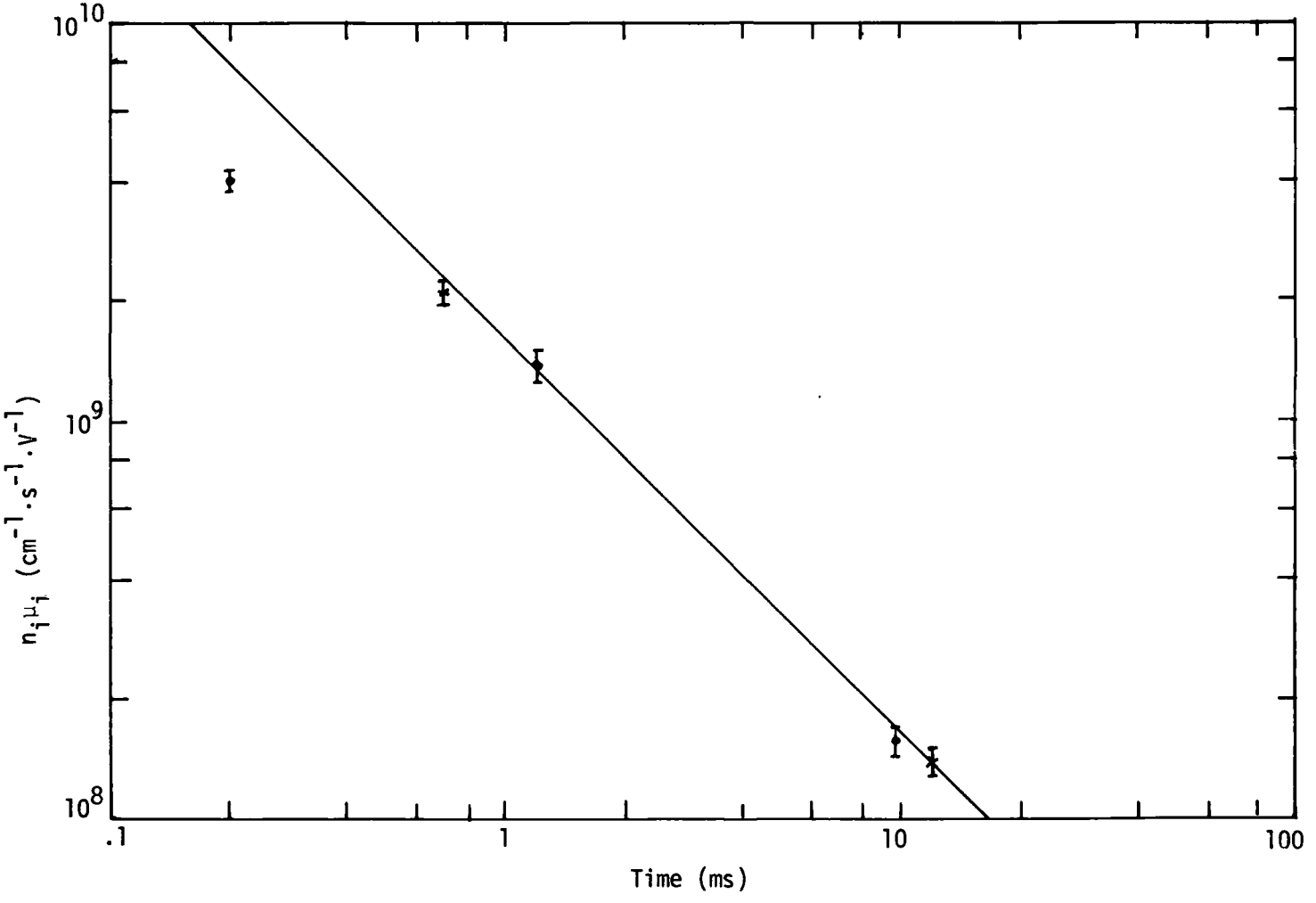

Figure 14. The product of remaining ions times mobility as a function of time. x's are for dry air, dots for wet (3% H_2O) air.

the mobilities measured before 1960 are suspect as measurements to be compared to theoretical calculations, (Ref. 11) the gas purity is probably comparable to that used in this experiment. Loeb (Ref. 12) quotes the results of Bradbury for room air to be 1.6 for the positive ion and 2.2 for the negative ion. Adopting a value of $\mu_i \approx 2$ cm^2/V·s and Sayers' value for β, the ratio $\mu_i/\beta = 9.1 \times 10^5$ cm^{-1}·V^{-1}, about 40% lower than our value. Since our value is measured at $\sim 50°C$ and Sayers value is at somewhat lower temperature (not specified by Sayers) and according to Thomson's theory $\beta \sim T^{-3/2}$, temperature difference accounts for part of the difference in the values of μ_i/β.

Data were also taken to measure the ion current at times after the Febetron was fired. The ion current measured in .27 atm of air are given in Table 4. Because of the much lower initial ion density compared to the HERMES data and limited range of the data the Febetron data is described by Equation (7) rather than Equation (13). Therefore, a value of μ_i/β cannot be found directly from the data. The increased current in dry air is consistent with the greater ion mobility measured in dry air compared to "wet" air. (Ref. 13)

4.3 IONIZATION ENHANCED BREAKDOWN

On 22 February 1980, after the goals of the late-time air chemistry experiment had been achieved, the HERMES II generator malfunctioned and was down for the rest of the day. This opportunity was used to study the electrical breakdown in air irradiated with the Febetron. It had been previously noted that a protective spark gap in the Febetron trigger circuit was breaking down at a much lower voltage than was expected. This occurred when the spark gap received about 1 rad from the HERMES produced Bremsstrahlung at up to 10 ms before the application of the voltage.

Table 4. Ion current at times after a Febetron shot.

DELAY (ms)	APPLIED VOLTAGE (V)	AMPLIFIER GAIN	ION CURRENT (μA)	GAS
0	500	10	14	0.27 atm air + 3% H_2O
0.94	500	10	13	0.27 atm air + 3% H_2O
0.94	1000	10	25	0.27 atm air + 3% H_2O
0.94	1000	10	25	0.27 atm air + 3% H_2O
9.90	1000	10	22	0.27 atm air + 3% H_2O
9.93	1000	10	20	0.27 atm air + 3% H_2O
0.45	1000	10	26	0.27 atm air + 3% H_2O
0.44	1000	10	28	0.26 atm dry air
1.04	1000	10	28	0.26 atm dry air

In order to go to higher values of E/O, and thus closer to breakdown conditions, the pressure in the ion chamber was reduced to about 1/4 atm. Breakdown was studied for both wet and dry air and for various delay times between the firing of the Febetron and the application of the voltage to the ion chamber plates. The experimental conditions and results are summarized in Table 5. When the applied voltage was 500 V the air in the chamber did not breakdown. When the applied voltage was 1000 V and the Febetron was fired after the voltage was applied (listed as a delay time of 0.) a breakdown always occured. When the Febetron was fired first followed by the application of the 1000 V, the occurrence of a breakdown depended upon the delay time: breakdown was not observed at a delay time of 10 ms; but was observed on some shots at all smaller delay times. The occurrence and characteristics (time of occurrence, size, etc.) of a breakdown were to some extent random as shown by different behavior for identical experimental conditions.

The voltage applied across the chamber gap is far below the breakdown voltage for air that has not been ionized. Figure 15 shows the Paschen curve of breakdown voltage in air for plane parallel electrodes (as in our chamber) versus the product of pressure and plate separation (Ref. 14). These data were taken with brass electrodes but the curve for aluminum should be similar. We were working at a value of Pd = .35 cm·atm, so the chamber should withstand a voltage of 10,000 V or more. (By extrapolating the curve of Figure 15 to larger values of Pd.) Since the chamber was not designed for breakdown studies it is possible that a shorter air path exists between the high voltage and ground than the plate gap. (This is especially likely around the vacuum feedthrough connector.) Even so, the Pachen curve indicates that at 1000 V and .25 atm a gap of .04 cm is required for breakdown and this is much smaller than inadvertant gaps in the chamber.

On the shots on which the voltage was applied before the Febetron, free electrons produced in the gap cause a large initial current which

Table 5. Breakdown experiments with Febetron

Shot Number	Applied Voltage (V)	Delay Time (ms)	Air	Breakdown time after voltage
B-16	1000	0	dry	immediate
B-17	1000	0	"	immediate & 100 ms
B-18	1000	0	"	immediate
B-19	500	0	"	no
B-20	500	0	"	no
B-21	500	0	"	no
B-22	500	.94	"	no
B-23	1000	.94	"	small at 260 μs
B-24	1000	.94	"	large at 290 μs & 1.7 ms
B-25	1000	9.90	"	no
B-26	1000	9.91	"	no
B-27	1000	9.93	"	no
B-28	10000	?	"	?
B-29	1000	.45	"	small at 100 μs
B-30	1000	.44	wet	no
B-31	1000	1.05	"	at 1.5 ms
B-32	1000	1.04	"	no
B-33	1000	1.04	"	no
B-34	10000	0	"	immediate

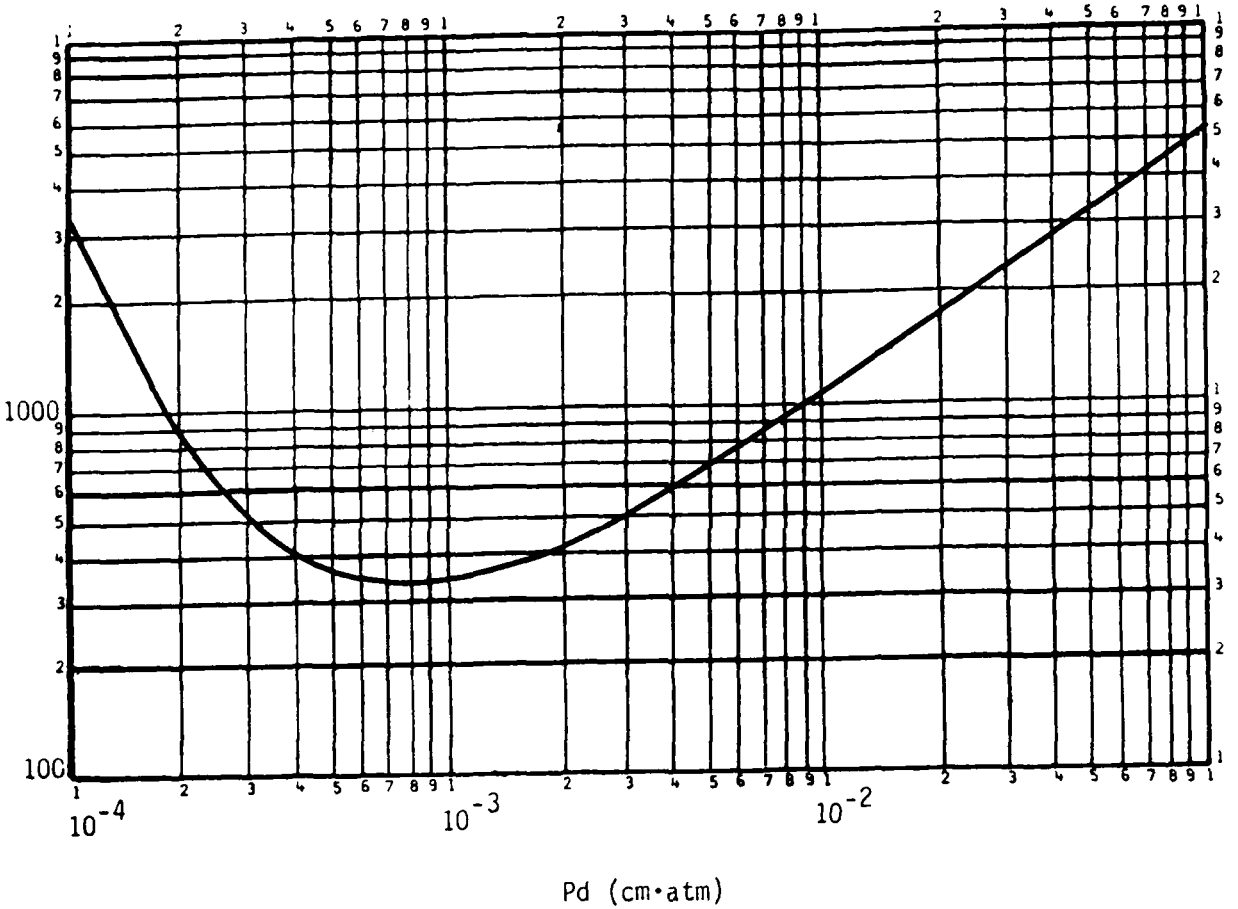

Figure 15. Paschen breakdown voltage.

initiates a self-sustaining breakdown. The mechanisms involved when the breakdown is initiated by radiation instead of high field are not well understood. One mechanism which explains the low sustaining voltages of gaseous breakdowns is that a region of large space charge density is formed in which the field is large enough to produce free electrons by impact multiplication. We can estimate the space charge of the electric field due to boundary layer formation in the ion chamber. At the applied field of 1000 V and pressure of .27 atm, the value of $E/P \approx 2550$ V/cm·atm, $\mu \approx 3000$ cm^2/V·s, and $\alpha \approx 1.2 \times 10^6$ s^{-1}. For a dose of 50 mrad the charge density of free electrons in the ion chamber is 5.6×10^{-12} C/cm^3. The attachment distance, $\mu E/\alpha$, is larger than the gap separation of 1.4 cm. Thus the maximum voltage dropped across the boundary layer is

$$\Delta V = \frac{1}{2} \frac{\rho}{\varepsilon_o} d^2 = 61 \text{ V} \qquad (16)$$

Thus space charge increase of the local field cannot explain the breakdown.

Even more surprising are the shots in which breakdown occurs when the voltage is applied after the free electrons produced by the radiation have attached to form negative ions. An additional mechanism is needed here to explain the initiation of the breakdown process. Detachment of electrons from the negative ions seems likely, but it is not understood how this comes about.

Oscilloscope photographs of the breakdown waveforms are shown in Figure 16. Figure 16a shows the immediate breakdown when the Febetron is fired into the charged plates. After recovery a high frequency oscillation sets in after ~ 800 μs. Figure 16b shows the breakdown when the voltage was applied .9 ms after the Febetron was fired. Approximately 300 μs after the switching transient a breakdown is observed. Again a oscillation occurs ~ 1 ms after recovery. This oscillation which appears to have a net negative current (it is centered below the baseline), may be artifact

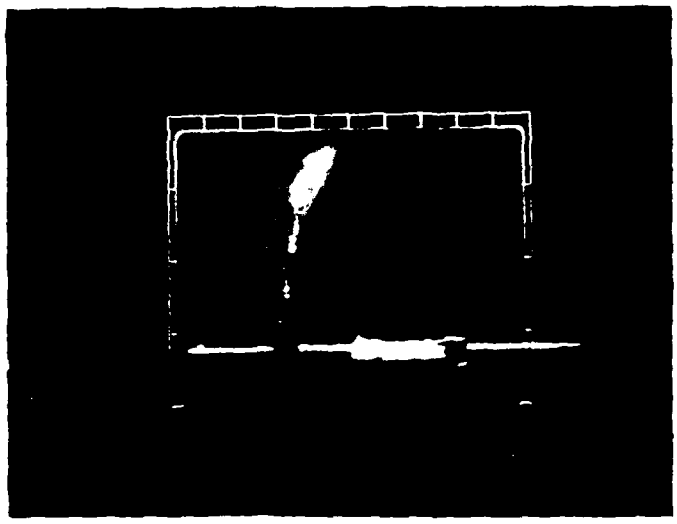

(enchanced)

a) Shot B-17. Immediate breakdown when Febetron is fired. Vertical scale 4 V/division, horizontal scale 500 μs/division.

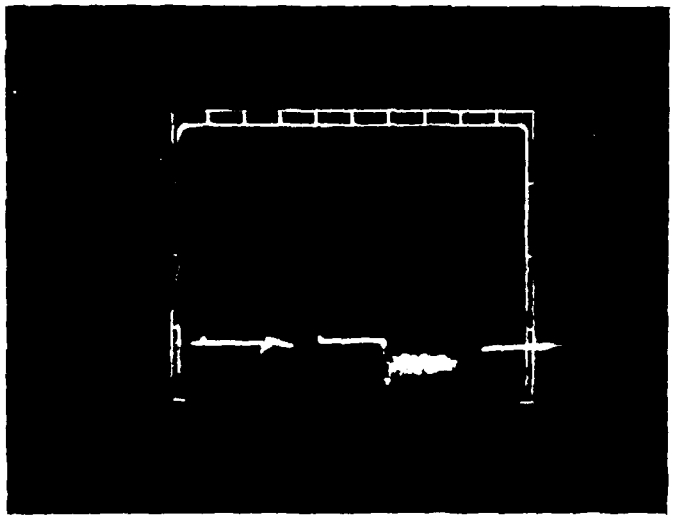

(enhanced)

b) Shot B-24. Breakdown 300 μs after voltage was applied. Febetron fired ~ 1 ms before voltage. Vertical scale 4 V/division, horizontal scale 500 μs/division.

Figure 16.

(enhanced)

c) Shot B-16. Immediate breakdown when Febetron is fired (50 μs after shunt across measuring resistor was removed). Vertical scale .4V/division, horizontal scale 50 μs/division.

(enhanced)

d) Shot B-29. Small discharge ~ 100 μs after shunt across measuring resistor was removed. Febetron fired ~ .5 ms before voltage was applied. Vertical scale .4V/division, horizontal scale 50 μs/division.

Figure 16. (continued)

of the electronics which was not designed to handle the large currents seen at breakdown. In Figure 16c and d breakdown waveforms are shown in an expanded time scale. Figure 16d shows a very small spike discharge containing less than .1 n C of charge.

Further experimentation with a better controlled geometry and extensive change of parameters such as dose, pressure, gap size, electrode material and gas composition is needed to gain an understanding of the effect of radiation on electrical breakdown.

SECTION 5

CONCLUSIONS

Although the chemical composition of highly dosed air may be quite different than undosed air, we find that the electron conductivity of both gases are the same to within the 20 percent accuracy of this experiment. The amount of HNO_3 or other highly attaching species formed in air with 3 percent water vapor by a dose of 2×10^6 rad was insufficient to change the attachment rate by more than 20 percent if the electron mobility remains constant. If the ionization smog formation in our ion chamber was the same as that after a nuclear burst, i.e. the chemical reactions are not dependent on having high energy electrons present except initially, then the discrepancy between the electric field used in source region EMP calculations and the existence of lightning cannot be explained on the basis of a lower electron conductivity in highly dosed air.

We found the ratio of the mobility to the ion-ion recombination coefficienty for highly dosed air to be 3.9×10^6 cm^{-1} V^{-1} at 1 atm pressure and $\sim 50°C$ in rough agreement with the value for undosed air.

We also found that [illegible]ation on the order of 50 mrad reduced the breakdown voltage across a 1.4 [illegible] by roughly a factor of 10. This ionization enhanced breakdown occurred even if the radiation was applied 1 ms before the voltage.

REFERENCES

1. Chervenak, J.G. "Late-Time Air Chemistry Experiments," Mission Research Corporation, MRC/SD-R-32, December 1978

2. Uman, M.A., D.F. Seacord, G.H. Price, and E.T. Pierce, JGR 77, 1592 (1972).

3. Scheibe, M., "The Increased Attachment Due to Ionization Induced Smog in EMP Environments," MRC-R-532, Mission Research Corporation, 1979.

4. Price, M.L., and V.A.J. van Lint, "Measurement of Electron Attachment and Mobility in Dry and Wet Air," DNA 4788T, Mission Research Corporation, December 1978.

5. The data shown in Figure 3 is courtesy of Sandia Laboratories.

6. Schuck, R.L., HERMES II Experimenter's Manual, Sandia Laboratories, Albuquerque, N.M., SAND77-0341, 1977.

7. The TLD data shown in Figure 10 is courtesy of Sandia Laboratories.

8. Pettus, E. and W.F. Crevier, "Analytic Representation of Electron Mobility and Attachment Data in Dry and Moist Air from van Lint's HIFX Experiments,", MRC-R-576, Mission Research Corporation, Santa Barbara, CA.

9. This fact was pointed out by Dr. Forrest Gilmore.

10. Sayers, J., Proc. Roy. Soc., A169, 83 (1938).

11. McDaniel, E.W. and E.A. Mason, The Mobility and Diffusion of Ions in Gases, John Wiley and Sons, p.v., 1973.

12. Loeb, L.B., "Basis Processes of Gaseous Electronics," University of California Press, p. 116, 1961.

13. Huxley, L.G. and R.W. Crompton, The Diffusion and Draft of Electrons in Gases, John Wiley and Sons, 3 (1974).

14. Papoular, R., Electrical Phenomena in Gases, American Elsevier Publishing Company, p. 110, 1965.

DISTRIBUTION LIST

DEPARTMENT OF DEFENSE

Assistant to the Secretary of Defense
Atomic Energy
ATTN: Executive Assistant

Defense Communications Agency
ATTN: Code C313
ATTN: Code 312

Defense Communications Engineer Center
ATTN: Code R720, C. Stansberry
ATTN: Code R123
ATTN: Code R400

Defense Intelligence Agency
ATTN: RDS-3A

Defense Nuclear Agency
2 cy ATTN: RAEE
4 cy ATTN: TITL

Defense Technical Information Center
12 cy ATTN: DD

Field Command
Defense Nuclear Agency
ATTN: FCLMC
ATTN: FCPR

Field Command
Defense Nuclear Agency
Livermore Branch
ATTN: FCPRL

Interservice Nuclear Weapons School
ATTN: TTV

Joint Chiefs of Staff
ATTN: J-3

Joint Strategic Tgt Planning Staff
ATTN: JSAS
ATTN: NRI-STINFO Library
ATTN: JPST
ATTN: JLA

National Communications System
ATTN: NCS-TS

National Security Agency
ATTN: S-232, D. Vincent
ATTN: R-52, O. Van Gunten

Under Secretary of Defense for Rsch & Engrg
ATTN: Strategic & Space Sys (OS)

DEPARTMENT OF THE ARMY

BMD Systems Command
Department of the Army
ATTN: BMDSC-HW, R. Dekalb
ATTN: BMDSC-AOLIB

U.S. Army Armor Center
ATTN: Technical Library

DEPARTMENT OF THE ARMY

Electronics Tech & Devices Lab
U.S. Army Electronics R&D Command
ATTN: DELCS-K, A. Cohen
ATTN: DELSD-L, W. Werk
ATTN: DRDCO-COM-ME, G. Gaule

Harry Diamond Laboratories
Department of the Army
ATTN: DELHD-N-EMA
ATTN: DELHD-N-EME
ATTN: DELHD-N-EMD
ATTN: DELHD-N-RB
ATTN: DELHD-N-EMB
ATTN: DELHD-N-EM, Chief EME Lab
ATTN: DELHD-N-RCC
2 cy ATTN: DELHD-N-RBC
ATTN: DELHD-N-EM-C
ATTN: DELHD-N-TD
ATTN: Chief, Div 10000
ATTN: DELHD-N-TF
ATTN: DELHD-I-TL

U.S. Army Ballistic Research Labs
ATTN: DRDAR-BLE
ATTN: DRDAR-BLB, W. Van Antwerp

U.S. Army Comm-Elec Engrg Instal Agency
ATTN: CCC-CED-SES

U.S. Army Communications Command
ATTN: CC-OPS-OS
ATTN: CC-OPS-PD
ATTN: ATSI-CD-MD

U.S. Army Communications Sys Agency
Department of the Army
ATTN: CCM-AD-SV
ATTN: CCM-RD-T

U.S. Army Electronics R&D Command
ATTN: DRDCO-SEI
ATTN: DRCPM-ATC

U.S. Army Engineer Div Huntsville
ATTN: HNDED-SR

U.S. Army Intel Threat Analysis Detachment
ATTN: Admin Officer

U.S. Army Intelligence & Sec Cmd
ATTN: Tech Info FAC
ATTN: Technical Library

U.S. Army Materiel Sys Analysis Actvy
ATTN: DRXSY-PO

U.S. Army Missile R&D Command
ATTN: DRDMI-EAA
ATTN: Documents Section
ATTN: DRCPM-PE-EA, W. Wagner
ATTN: DRCPM-PE-EG, W. Johnson

U.S. Army Training and Doctrine Comd
ATTN: ATCD-Z

DEPARTMENT OF THE ARMY (Continued)

U.S. Army Test and Evaluation Comd
ATTN: DRSTE-EL
ATTN: DRSTE-FA

White Sands Missile Range
Department of the Army
ATTN: STEWS-TE-AN, J. Okuma

DEPARTMENT OF THE NAVY

Naval Air Systems Command
ATTN: AIR 350F

Naval Construction Battalion Center
ATTN: Code L08A

Naval Electronic Systems Command
ATTN: PME 117-21

Naval Ocean Systems Center
ATTN: Code 08, J. Rockway
ATTN: Code 8123, S. Lichtman
ATTN: Code 54, C. Fletcher

Naval Ordnance Station
ATTN: Standardization Division

Naval Postgraduate School
ATTN: Code 1424, Library

Naval Research Laboratory
ATTN: Code 2627, D. Folen
ATTN: Code 1434, E. Brancato
ATTN: Code 6624
ATTN: Code 6623, R. Statler

Naval Surface Weapons Center
White Oak Laboratory
ATTN: Code F30
ATTN: Code F32, E. Rathbun

Naval Surface Weapons Center
ATTN: Code F-56

Naval Weapons Center
ATTN: Code 233

Naval Weapons Evaluation Facility
ATTN: Code AT-6

Office of Naval Research
ATTN: Code 427

Strategic Systems Project Office
Department of the Navy
ATTN: NSP-43
ATTN: NSP-2342, R. Coleman
ATTN: NSP-2701, J. Pitsenberger
ATTN: NSP-27334
ATTN: NSP-230, D. Gold

DEPARTMENT OF THE AIR FORCE

Aeronautical Systems Division
Air Force Systems Command
ATTN: ASD/YYEF
ATTN: ASD/ENETV
ATTN: ASD/ENAMA, J. Corbin

DEPARTMENT OF THE AIR FORCE (Continued)

Air Force Technical Applications Ctr
ATTN: TFS, M. Schneider

Air Force Weapons Laboratory
Air Force Systems Command
ATTN: NT
ATTN: ELT, W. Page
ATTN: CA
ATTN: EL, C. Baum
ATTN: ELXT
ATTN: NTN
ATTN: SUL
ATTN: ELA, J. Castillo
ATTN: NXS
ATTN: ELP

Air Logistics Command
Department of the Air Force
ATTN: OO-ALC/MMETH, P. Berthel
ATTN: OO-ALC/MM, R. Blackburn
ATTN: OO-ALC/MMEDO, L. Kidman

Air University Library
Department of the Air Force
ATTN: AUL-LSE

Ballistic Missile Office
Air Force Systems Command
ATTN: MNNXH, J. Allen
ATTN: MNNH, J. Tucker

Electronic Systems Divison
ATTN: YSEA

Foreign Technology Division
Air Force Systems Command
ATTN: NIIS Library
ATTN: TQTD, B. Ballard

Headquarters Space Division
Air Force Systems Command
ATTN: IND

Headquarters Space
Air Force Systems Command
ATTN: YAPC

Rome Air Development Center
Air Force Systems Command
ATTN: TSLD

Sacramento Air Logistics Center
Department of the Air Force
ATTN: MMIRA, J. Demes
ATTN: MMSREM, F. Spear
ATTN: MMCRS, H. Delmastro

Strategic Air Command
Department of the Air Force
ATTN: XPFS, B. Stephan
ATTN: NRI-STINFO Library
ATTN: NRI, G. Matzke
ATTN: DEL

DEPARTMENT OF ENERGY

Department of Energy
Albuquerque Operations Office
ATTN: CTID
ATTN: WSSB

Department of Energy
Economic Regulatory Administration
ATTN: Office of Utility Systems, L. O'Neill

OTHER GOVERNMENT AGENCIES

Central Intelligence Agency
ATTN: OSWR/NED

Department of Transportation
Federal Aviation Administration
ATTN: Sec Div, ASE-300

Federal Emergency Management Agency
ATTN: Plans & Operations (EO)
ATTN: Plans & Operations (SE)

Federal Preparedness Agency
ATTN: ESTE, M. Murtha

DEPARTMENT OF ENERGY CONTRACTORS

Lawrence Livermore National Lab
ATTN: Tech Info Dept Library
ATTN: L-153, D. Meeker
ATTN: L-96, T. Donich
ATTN: L-156, E. Miller
ATTN: L-156, H. Cabayan
ATTN: L-10, H. Kruger

Los Alamos National Scientific Lab
ATTN: C. Benton
ATTN: B. Noel
ATTN: MS 670, J. Hopkins

Sandia National Lab
ATTN: R. Parker
ATTN: C. Vittitoe
ATTN: E. Hartman

DEPARTMENT OF DEFENSE CONTRACTORS

Aerospace Corp
ATTN: C. Greenhow
ATTN: J. Reinheimer
ATTN: I. Garfunkel
ATTN: Library
ATTN: C. Pearlston

Agbabian Associates
ATTN: Library

AVCO Research & Systems Group
ATTN: Library A830

Battelle Memorial Institute
ATTN: E. Leach

BDM Corp
ATTN: Corporate Library

BDM Corp
ATTN: Library

DEPARTMENT OF DEFENSE CONTRACTORS (Continued)

Bendix Corp
ATTN: M. Frank

Bendix Corp
ATTN: Dept 6401

Boeing Co
ATTN: Kent Tech Library
ATTN: D. Kemle
ATTN: H. Wicklein
ATTN: V. Jones
ATTN: B. Hanrahan

Boeing Wichita Co
ATTN: L. Weller

Booz-Allen and Hamilton, Inc
ATTN: Tech Library
ATTN: R. Chrisner

Calspan Corp
ATTN: Library

Charles Stark Draper Lab, Inc
ATTN: K. Fertig
ATTN: TIC MS 74

Cincinnati Electronics Corp
ATTN: L. Hammond

Computer Sciences Corp
ATTN: R. Briggs

Computer Sciences Corp
ATTN: A. Schiff

Cutler-Hammer, Inc
ATTN: E. Karpen

Dikewood Corporation
ATTN: Tech Library
ATTN: L. Davis

Dikewood Corporation
ATTN: K. Lee

Douglas Aircraft Company
ATTN: M. Potter

E-Systems, Inc
ATTN: J. Moore

Effects Technology, Inc
ATTN: Tech Info Acq, S. Clow

EG&G Wash Analytical Svcs Ctr, Inc
ATTN: C. Giles

Electro-Magnetic Applications, Inc
ATTN: D. Merewether

Ford Aerospace & Communications Corp
ATTN: K. Attinger
ATTN: E. Poncelet, Jr

Franklin Institute
ATTN: R. Thompson

DEPARTMENT OF DEFENSE CONTRACTORS (Continued)

General Dynamics Corp
Electronics Division
ATTN: Research Library

General Dynamics Corp
ATTN: Research Library

General Electric Co
ATTN: C. Hewison

General Electric Co
ATTN: Technical Library

General Research Corp
3 cy ATTN: Tech Info Office

Georgia Institute of Technology
ATTN: R. Curry

Georgia Institute of Technology
ATTN: Res & Sec Coord for H. Denny

Grumman Aerospace Corp
ATTN: L-01 35

Harris Corporation
ATTN: V. Pres & Mgr Prgms Div

Hazeltine Corp
ATTN: J. Okrent

Honeywell, Inc
ATTN: R. Johnson
ATTN: S&RC Library

Honeywell, Inc
ATTN: W. Stewart
ATTN: S. Graff

Horizons Technology, Inc
ATTN: R. Kruger

Hughes Aircraft Co
ATTN: J. Singletary
ATTN: K. Walker
ATTN: CTDC 6/E110

Hughes Aircraft Co
ATTN: A. Narevsky

Hughes Aircraft Co
ATTN: K. Downing MLS 100

IIT Research Institute
ATTN: ACOAT

IIT Research Institute
ATTN: I. Mindel
ATTN: J. Bridges

Institute for Defense Analyses
ATTN: Tech Info Services

International Tel & Telegraph Corp
ATTN: A. Richardson
ATTN: Tech Library

JAYCOR
ATTN: W. Radasky

DEPARTMENT OF DEFENSE CONTRACTORS (Continued)

IRT Corp
ATTN: B. Williams
ATTN: N. Rudie

JAYCOR
ATTN: R. Stahl
ATTN: E. Wenaas

JAYCOR
ATTN: Library

Kaman Sciences Corp
ATTN: F. Shelton
ATTN: A. Bridges
ATTN: W. Rich
ATTN: N. Beauchamp

Kaman TEMPO
ATTN: R. Rutherford
ATTN: DASIAC
ATTN: W. McNamara

Kaman TEMPO
ATTN: DASIAC

Litton Systems, Inc
ATTN: M848-61
ATTN: EMC GP

Litton Systems, Inc
ATTN: J. Skaggs

Lockheed Missiles & Space Co., Inc
ATTN: Tech Info Center

Lockheed Missiles & Space Co., Inc
ATTN: H. Thayn
ATTN: G. Heath
ATTN: B. Kimura
ATTN: L. Rossi
ATTN: S. Taimuty

Lutech, Inc
ATTN: F. Tesche

M.I.T. Lincoln Lab
ATTN: L. Loughlin

Martin Marietta Corp
2 cy ATTN: M. Griffith

Martin Marietta Corp
ATTN: G. Freyer

McDonnell Douglas Corp
ATTN: T. Ender

McDonnell Douglas Corp
ATTN: S. Schneider

Mission Research Corp
ATTN: J. Lubell
ATTN: EMP Group
2 cy ATTN: C. Longmire
5 cy ATTN: Document Control

Mission Research Corp
ATTN: L. McCormick
ATTN: A. Chodorow

DEPARTMENT OF DEFENSE CONTRACTORS (Continued)

Mission Research Corp
4 cy ATTN: V. Van Lint
4 cy ATTN: J. Chervenak
5 cy ATTN: Document Library

Mission Research Corporation
ATTN: W. Stark

Mitre Corp
ATTN: M. Fitzgerald

Norden Systems, Inc
ATTN: D. Longo
ATTN: Tech Library

Northrop Corp
ATTN: RAD Effects GRP
ATTN: Lew Smith
ATTN: V. Demartino

Pacific-Sierra Research Corp
ATTN: H. Brode

Physics International Co
ATTN: Document Control

R & D Associates
ATTN: Document Control
ATTN: R. Schaefer
ATTN: C. Mo
ATTN: M. Grover
ATTN: P. Haas

R & D Associates
ATTN: J. Bombardt

Rand Corp
ATTN: W. Sollfrey
ATTN: LIB-D

Raytheon Co
ATTN: G. Joshi

Raytheon Co
ATTN: H. Flescher

RCA Corp
ATTN: G. Brucker

RCA Corp
ATTN: D. O'Connor
ATTN: L. Minich

Rockwell International Corp
ATTN: D-243-068, 031-CA31
ATTN: N. Rudie
ATTN: J. Monroe
ATTN: V. Michel

Rockwell International Corp
ATTN: B. White

Rockwell International Corp
ATTN: B-1 Div, TIC

Rockwell International Corp
ATTN: F. Shaw

DEPARTMENT OF DEFENSE CONTRACTORS (Continued)

Sanders Associates, Inc
ATTN: R. Despathy

Science Applications, Inc
ATTN: R. Parkinson

Science Applications, Inc
ATTN: N. Byrn

Science Applications, Inc
ATTN: W. Chadsey

Sidney Frankel & Associates
ATTN: S. Frankel

Singer Co
ATTN: Tech Info Center

Sperry Rand Corp
ATTN: M. Cort

Sperry Rand Corp
ATTN: Tech Library

Sperry Rand Corp
ATTN: D. Schow

Spire Corp
ATTN: R. Little

SRI International
ATTN: A. Whitson
ATTN: B. Gasten

Sylvania Systems Group
ATTN: C. Thornhill
ATTN: L. Blaisdell

Sylvania Systems Group
ATTN: C. Ramsbottom
ATTN: D. Flood
ATTN: J. Waldron
ATTN: E. Motchok
ATTN: M. Nurefora
ATTN: A. Novemski

Systems, Science & Software, Inc
ATTN: A. Wilson

Teledyne Brown Engineering
ATTN: F. Leonard

Texas Instruments, Inc
ATTN: D. Manus
ATTN: Tech Library

Texas Tech University
ATTN: T. Simpson

TRW Defense & Space Sys Group
ATTN: W. Gargaro
ATTN: R. Plebuch
ATTN: L. Magnolia
ATTN: O. Adams
ATTN: H. Holloway

DEPARTMENT OF DEFENSE CONTRACTORS (Continued)

United Technologies Corp
ATTN: Chief Elec Design

DEPARTMENT OF DEFENSE CONTRACTORS (Continued)

Westinghouse Electric Corp
ATTN: Technical Library


DATE
ILME